

LATE EOCENE TERRESTRIAL PALEOCLIMATE RECORD FROM THE WHITE
RIVER FORMATION AT FLAGSTAFF RIM, WYOMING, USA

A Thesis
Submitted to
The Temple University Graduate Board

In Partial Fulfillment
Of the Requirements for the Degree
MASTER OF SCIENCE

By
Neil Patrick Griffis
January 2011

Dr. Dennis O. Terry, Jr. Thesis Advisor

Dr. David E. Grandstaff

Dr. Allison Tumarkin-Deratzian

ABSTRACT

Flagstaff Rim near Casper, WY preserves the most complete late Eocene section of the White River Group with over 219 m of late Eocene age sediment compared to 35 m preserved at Toadstool Park, NE. While Flagstaff Rim does not span the Eocene-Oligocene transition, it holds the earliest clues in the White River Group of a late Eocene (37-34 Ma) climatic deterioration. In this study 8 paleosols were collected, described and analyzed based on pedogenic features, mineralogy, and geochemistry, above and below dated volcanic ash beds. The lowermost paleosol is composed of smectite- rich red mudstone, with greenish gray drab haloes, and weather into hummocks. The sediments within this part of the section are the lithologic equivalent of the Peanut Peak member of Toadstool Park, NE and reflect a moist humid environment. Overlying these sediments is the lithologic equivalent of the Big Cottonwood Creek member. These sediments are comprised of smectite poor mudstones and yellow/beige sandstones, are indurated with calcium carbonate, and reflect a more arid environment. The transitional zone between the Peanut Peak and Big Cottonwood Creek lithologies corresponds with an increase in volcanism from the Great Basin, impact events, and building of ephemeral glaciers on Antarctica. The impact events and increase in volcanism, while synchronous with the transitional zone between the Peanut Peak and Big Cottonwood Creek lithologies, cannot explain the long term climatic perturbation, which persists within the White River Group. Instead, the climatic deterioration is likely explained by the building of ephemeral Antarctic ice sheets, which was compounded by the increase in volcanism and impacts. Regional variations in $\delta^{18}\text{O}$ isotopes within the White River Group can likely explain the suggested variations in paleoclimate across the Eocene-Oligocene transition.

Dedicated to Terrence McCann and His Family

ACKNOWLEDGEMENTS

Dr. Dennis Terry (DT) - First and foremost, thank you for the amount of time and work you have invested into my education. There has never been a time that I could not go into your office to ask a question or reason through a problem with you; you have always been there for me (even on sabbatical) and for that I am extremely grateful. The educational and life experiences I have gained under your study will stay with me for the rest of my life. The time spent in the Badlands of Nebraska and Wyoming in the 90 degree summer heat, the Frontier Bar and the moment where I had one foot on a cliff face the other almost in the mouth of a “prairie rattler” are a just of few of the many unforgettable experiences that I endured under your study. Thank you.

Dr. Grandstaff (G) - I will never forget your love for Celsius. You have taught me so much about geochemistry and more importantly that there was so much I did not know about geochemistry. You have really been an excellent and unforgettable teacher as well as a second advisor over my last semester at Temple.

Dr. Allison – I have learned so much from you both as a student in your class as well as being your lab instructor. Your vertebrate paleontology class was awesome!

Dr. Nyquist - I now am prepared to beat anyone I play in chess.

Temple geology faculty – You have made my time at Temple an unforgettable experience. I now feel confident in my abilities as a geologist thanks to all of you.

Shelah- I never would have never gotten as far as I have, had it not been your constant support and motivation. You have brightened my cloudiest days at Temple.

Steve Peterson – You’re the man! Thank you for all the time you spent running my samples through the XRD.

Raymond Kennedy – I will never forget the times we spent in the field. You have taught me so much about soils and have always been there to talk.

Graduate Colleagues- I enjoyed all the time we have spent together.

Friends and Family- Thank you for your continued support throughout my college career. Mom and Dad thank you, I love you both. Granny, you have been there since day one. Martin, you have always been there to both talk and listen. Sarah, I can’t imagine how difficult it must have been to hear me talk nonstop about paleopedology and sedimentary geology, thank you for your support.

TABLE OF CONTENTS

	Page
ABSTRACT.	ii
DEDICATION.	iii
ACKNOWLEDGMENTS.	iv
LIST OF TABLES.	vii
LIST OF FIGURES.	viii
CHAPTER	
1. INTRODUCTION.	1
1.1. Eocene-Oligocene Transition.....	1
1.2. Geologic Background.....	4
1.3. Previous Work.....	9
1.4. Stratigraphic Correlations.....	10
2. MATERIALS AND METHODS.	12
2.1. Field and Microscope Analysis.....	12
2.2. Geochemical Analysis.....	12
2.3. Classification.....	15
3. RESULTS.	16
3.1. Paleosols.....	16
3.1.1. <i>Tipps Trench Paleosol</i>	16
3.1.2 <i>Ash A Paleosols</i>	22
3.1.3. <i>Ash B Paleosol</i>	25
3.1.4 <i>Ash F Paleosols</i>	27

3.1.5 <i>Ash J Paleosols</i>	30
4. DISCUSSION.....	33
4.1. Soil Formation.....	33
4.1.1. <i>Climate</i>	33
4.1.2. <i>Organisms</i>	36
4.1.3. <i>Relief</i>	37
4.1.4. <i>Parent Material</i>	39
4.1.5. <i>Time</i>	42
4.2. Climate vs. Sedimentation Rates.....	43
4.3. Regional Variations.....	44
5. CONCLUSION.....	47
REFERENCES CITED.....	49
APPENDIX	
Geochemical Data	

LIST OF TABLES

Table 2.1 Molecular Weathering Ratios.....	14
Table 2.2 Paleoclimatic Proxies.....	15
Table 3.1 Tipps Trench Paleosol description.....	19
Table 3.2 Ash A Paleosol description.....	24
Table 3.3 Ash B Paleosol description.....	26
Table 3.4 Ash F Paleosol description.....	29
Table 3.5 Ash J Paleosol description.....	32

LIST OF FIGURES

Figure 1.1 Outcrops of the White River Group.....	5
Figure 1.2 Photographs of Flagstaff Rim, WY.....	7
Figure 1.3 Measured section of the White River Sequence at Flagstaff Rim, WY.....	8
Figure 1.4 Regional Stratigraphy between WY and NE.....	11
Figure 3.1 Measured sections and geochemistry of paleosol profiles.....	17
Figure 3.2 Photomicrographs of pedogenic features.....	20
Figure 3.3 XRD patterns from B horizons of individual paleosol profiles.....	21
Figure 4.1 Variations in MAP and MAT in paleosols.....	34
Figure 4.2 Provenance of Flagstaff Rim sediments.....	40
Figure 4.3 Sedimentation rates at Flagstaff Rim, WY.....	41
Figure 4.4 Current $\delta^{18}\text{O}$ variations of rainwater.....	45

Chapter 1: Introduction

1.1. Eocene-Oligocene Transition

The Eocene-Oligocene Transition (EOT) is recognized as a global shift from the “greenhouse” conditions of the Cretaceous and Paleogene to the “icehouse” of the Neogene and is considered to be the most dramatic climate change event of the Cenozoic (Miller et al., 1991; Coccioni et al., 2009; Terry, 2001). The Eocene-Oligocene boundary is defined in marine sections by the extinction of the planktonic foraminifera family Hantkeninidae from the Global Boundary Stratotype Section and Point (GSSP) at Massignano, Italy and is currently fixed at 33.91 ± 0.05 Ma (Brown et al., 2009; Alvarez et al., 2009; Hilgen and Kuiper 2009; Premoli Silva and Jenkins, 1993). In the terrestrial realm the Eocene-Oligocene boundary is slightly older than the Chadronian-Orellan “North American Land Mammal Age” boundary at ~ 33.7 Ma (Terry, 2001; Zanazzi et al., 2009). While the Eocene-Oligocene boundary and associated paleoclimate and paleoecological patterns are well studied in the marine realm, questions still remain surrounding the terrestrial response. Terrestrial and marine isotope records suggest that the EOT event was not synchronous, with terrestrial cooling occurring at ~ 33.7 Ma and the marine record showing cooling from ~ 33.7 - 33.4 Ma (Sheldon and Retallack, 2004). In late Eocene marine settings, a progressive turnover of coccolithophores occurred over a > 6 Ma time period with major extinctions occurring 34.2 Ma in the mid- and low-latitudes and 32.3 Ma at high-latitudes, as a result of both climatic cooling and the establishment of Antarctic ice sheets (Aubrey and Bord, 2009). Climatic perturbations have been associated with the Chesapeake Bay and Popigai impacts during the late Eocene, which occurred at 35.7 ± 0.2 in chron 16n.2 and at 35.5 ± 0.3 Ma, in chron

16n.1, respectively (Bottomley et al., 1997; Poag et al., 2004; Coccioni et al., 2009; Koeberl, 2009). A decrease of 2.5°C has been inferred in deep marine sediments based on Ca/Mg paleothermometry accompanied by a positive shift in $\delta^{18}\text{O}$ isotopes associated with Eocene – Oligocene Transition Event -1 (EOT-1) at 33.8 Ma, and the oxygen isotope excursion (Oi-1) at 33.55 Ma (Miller et al., 2009). The positive shift in $\delta^{18}\text{O}$ isotopes is thought to reflect the formation of Antarctic ice sheets. $\delta^{18}\text{O}$ and $\delta^{13}\text{C}$ patterns observed in middle Eocene marine sediments by McGowran (1989) and McGowran et al. (1992), are similar to those of the middle Miocene, which are thought to reflect the building of the modern Antarctic ice sheets (Prothero, 1992).

Within the terrestrial realm, $\delta^{18}\text{O}$ and $\delta^{13}\text{C}$ isotope compositions in fossil teeth and bones suggest a major drop of $7.1 \pm 3.1^\circ\text{C}$ over 400,000 years (Zanazzi et al., 2007, 2009). Leaf margin analysis indicates a drop of up to 13°C across the EOT (Wolfe, 1978). Fossil snails from the late Eocene, similar to those found in moist tropical climates, are replaced in the early Oligocene by small, compact gastropods, similar to those found today in more arid regions (Evanoff et al., 1992; Prothero, 2004). Oxygen isotopes obtained from tooth enamel phosphate of late Eocene-Oligocene horses suggest a possible increase in seasonality of temperature (Bryant et al., 1996). Climatic models obtained from paleosols suggest a long-term climate forcing and/or stepwise changes during the late Eocene versus one abrupt climate-forcing event (Sheldon and Retallack, 2004). Other paleosol climate models implicate the building of glaciers on Antarctica, which is thought to be reflected by Oi-1, as well as the establishment of the Cascade Range, as the main forcing mechanisms contributing to the aridification of North America (Sheldon, 2009).

Although climate perturbations appear to have been significant, the terrestrial Eocene-Oligocene boundary is not associated with any great mass extinction between the Chadronian and Orellan North American Land Mammal Ages (Evanoff et al., 1992). Even though there is no distinct climatic event which leads to the EOT, many climate changing events occur prior to the EOT, which makes the study of the late Eocene significant. Inconsistencies between the marine and terrestrial realm, as well as a dearth of terrestrial data, indicate the need for a more complete study of late Eocene terrestrial systems leading up to the Eocene-Oligocene boundary.

This paper provides a detailed analysis of 8 late Eocene (37-34 Ma) paleosols from the White River Formation¹ at Flagstaff Rim, Wyoming. Although the tephro-, bio- and magnetostratigraphy for this area are well documented and allow for large-scale regional correlation of the White River Group (WRG) (Prothero and Swisher, 1992), a paleoenvironmental reconstruction of the Flagstaff Rim exposures using fossil soils (paleosols) has yet to be attempted. Paleosols provide an excellent proxy for ancient climates and environments because their morphology, mineralogy and chemistry are dependent on the climatic and environmental conditions at the time of formation (Sheldon, 2009; Sheldon and Tabor, 2009). Paleotemperature, paleoprecipitation, paleofloras, and landscape stability can all be inferred based upon the macromorphologic, petrographic and geochemical evidence found within paleosols (Retallack, 1983; Terry and Evans, 1994; Terry, 2001; Sheldon and Retallack, 2004; Sheldon and Tabor, 2009). When placed within a geochronologic context, paleosols at Flagstaff Rim can aid in a terrestrial paleoclimatic reconstruction of the late Eocene.

¹ At Flagstaff Rim the White River strata are referred to as a formation (Emry, 1973), but for the purpose of this paper all strata will be referred to as part of the White River Group.

1.2. Geologic Background

The Eocene-Oligocene Boundary is preserved at various locations within the WRG of South Dakota, North Dakota, Wyoming, Colorado and Nebraska (Fig. 1.1). The Eocene-Oligocene WRG is a volcanoclastic and siliciclastic sequence composed of claystones, siltstones, sandstones and limestones deposited in fluvial, lacustrine and eolian environments (Darton, 1908; Schultz and Stout, 1955; Emry, 1973; Terry, 2001). The WRG is thickest in Wyoming and Nebraska and thins to the northeast toward North Dakota (Terry, 2001). Provenance studies of WRG tuffs point to the Great Basin of eastern Nevada and western Utah as the main source of volcanoclastic sediment based upon composition and timing (Larson and Evanoff, 1998). The most complete terrestrial late Eocene record of the WRG is located at Flagstaff Rim, WY, in Natrona County 5 miles northwest of the town of Alcova and 25 miles southwest of Casper, WY (Fig. 1.1). The corners of the Benton Basin, Benton Basin N.E., Clarkson Hill and Alcova USGS 7.5 minute Quadrangles make up the area referred to as Flagstaff Rim (Emry, 1973).

Current paleoclimatic models suggest the WRG records a change from sub-humid forested conditions to sub-arid environments dominated by shrubs and grass-like vegetation by the late Eocene. This change in climate is recognized by a change in clay mineralogy and a decrease in paleosol development (Terry and LaGarry, 1998; Terry, 2001). The interpreted decrease in precipitation occurred as part of an overall west to east drying trend throughout the WRG, which is recognized as a change from fluvial to fluvial plus eolian depositional systems (Evanoff et al., 1992; Terry, 2001).

The last 2.5 million years of the late Eocene is represented by the Peanut Peak and Big Cottonwood Creek Members of the WRG in Nebraska (Terry and LaGarry, 1998).

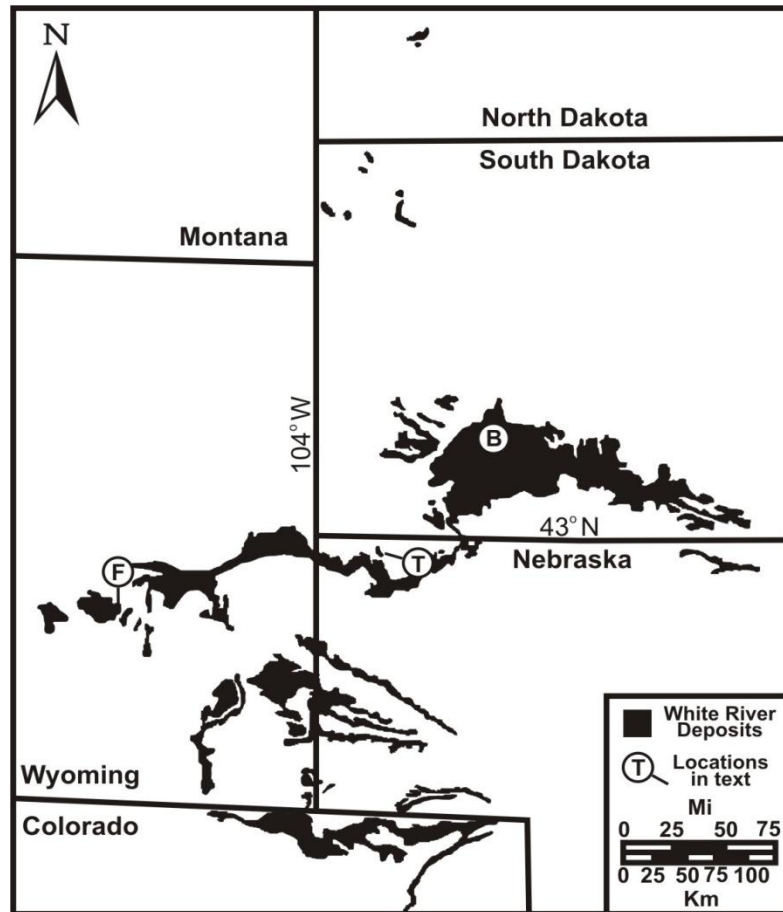


Figure 1.1. Outcrops of the White River Group. F – Flagstaff Rim, T- Toadstool Park, B- Badlands National Park. Modified from Terry (2001).

The Peanut Peak Member is recognized as a smectite-rich, bluish-green mudstone and claystone that weathers into hummocks (Fig. 1.2a). The Big Cottonwood Creek Member is composed of volcanoclastic overbank silty, claystones interbedded with tabular and lenticular channel sandstones and is more resistant to weathering (Fig. 1.2b, c; Terry, 1998; Terry and LaGarry, 1998). At Flagstaff Rim, the section has not been divided into formal members. For this reason strata at Flagstaff Rim are referred to with respect to rocks of similar lithologies in Nebraska.

Flagstaff Rim is comprised of 219 m of late Eocene tuffaceous strata (Fig 1.3), compared with roughly 35 m of temporally equivalent strata at Toadstool Geologic Park in northwest Nebraska (Fig. 1.1). In general, sediments become coarser westward within the WRG, due to greater proximity to the volcanic source area, although local Laramide uplifts provide significant siliciclastic components (Emry, 1973). The base of the section at Flagstaff Rim is composed of coarse conglomerate and boulders up to 1.5 m in diameter within an arkosic sandstone matrix. This in turn is overlain by variegated red, oxidized overbank mudstone with bands of reduced green sandstone and white channel sandstone, all of which weather into large “hummocks”. Mixed within the sandstone and claystone are bands of boulder conglomerates which were eroded from local highs (Emry, 1973). The sediments at the base of the Flagstaff Rim area are interpreted as a fluvial dominated depositional system (Evanoff et al., 1992). Moving up section, the sediments become more resistant and undergo a color change, with dark brown silt/claystone and yellowish sandstone common. These sediments overall are less weathered, less clay rich, and increasingly indurated with carbonate, resulting in a resistant, cliff-forming morphology (Fig.1.2c). The transition from the variegated red

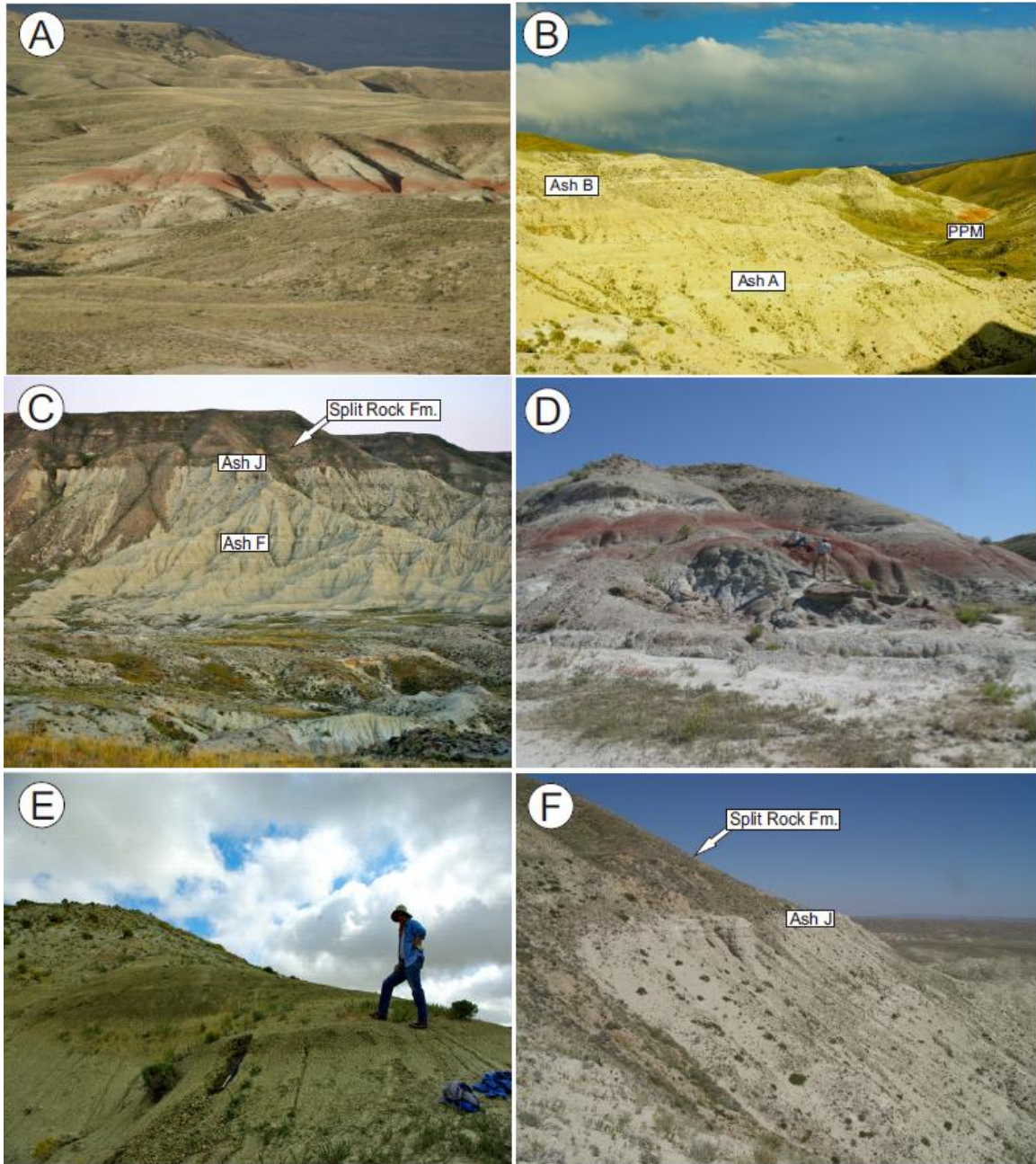


Figure 1.2 Outcrop photographs of Flagstaff Rim, WY: (A) Peanut Peak lithology at Flagstaff Rim, WY. Note the rounded hummocky nature of the sediments. (B) Ash A and B are within the transitional lithology. Note the difference between transitional lithology and the Peanut Peak lithology in the background (PPM). (C) The Big Cottonwood Creek lithology at Flagstaff Rim, WY, which tends to be more “cliff forming”. The Miocene Split Rock Formation, Ash F, and J are labeled. (D) The Tipps Trench paleosol locality within the Peanut Peak lithology. (E) The Ash B paleosol locality. Note the dark band which pinches out to the left and right. (F) The approximate location of Ash J paleosol locality within the Big Cottonwood Creek lithology. The Miocene Split Rock Formation and Ash J are labeled.

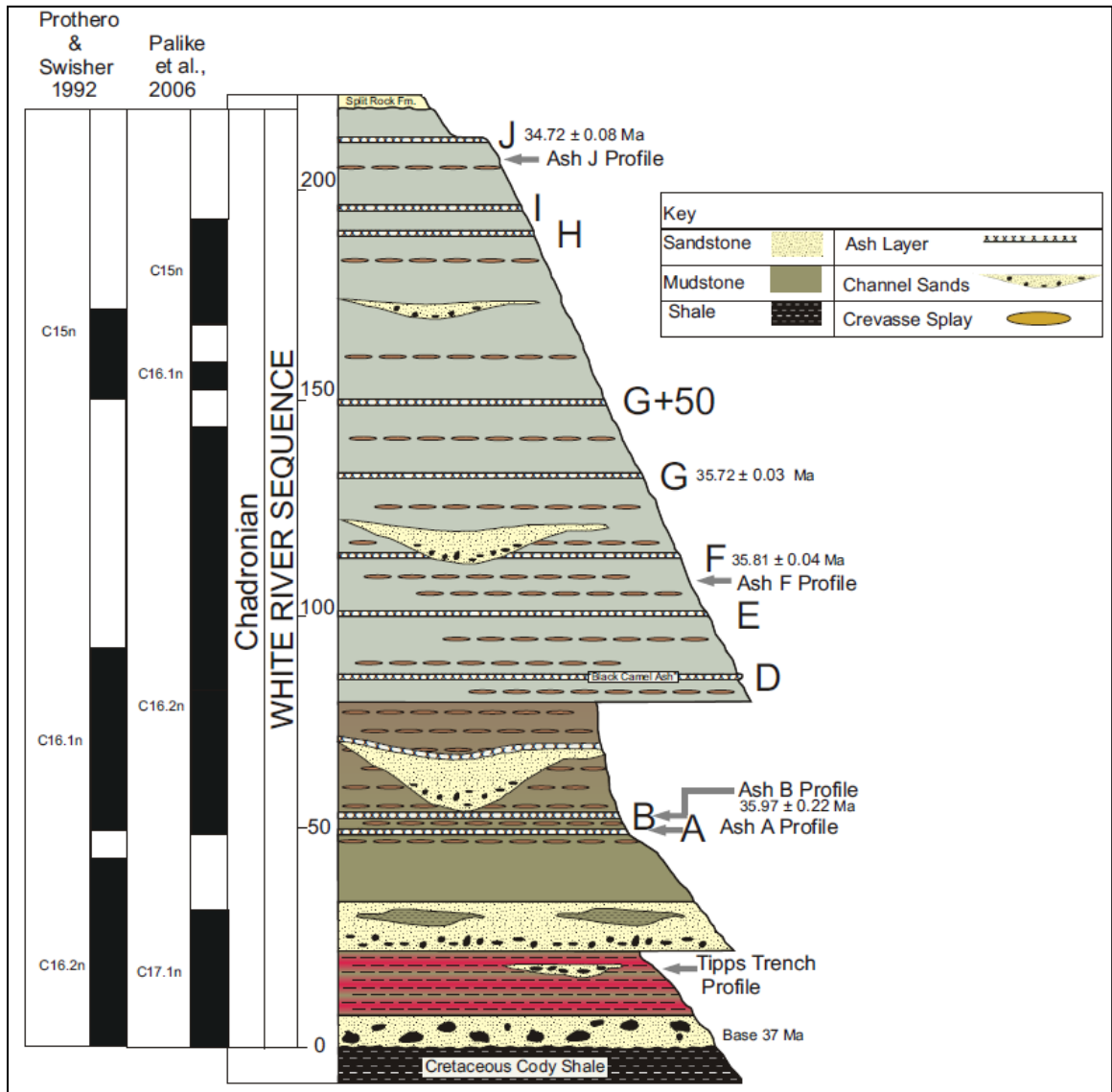


Figure 1.3. Measured section of the White River Sequence at Flagstaff Rim, WY modified from Emry (1973). Arrows indicate locations of paleosol trenches. Ash dates obtained using single-crystal $^{40}\text{Ar}/^{39}\text{Ar}$ analysis of anorthoclase and biotite by Prothero and Swisher (1992). Chron and Polarity reflect those of Prothero and Swisher (1992), compared to the astronomical polarity time scale (APTS06) of Palike et al. (2006).

and olive green sediments to the dark brown silt/claytone and yellowish sandstone is similar to the change from the Peanut Peak to Big Cottonwood Creek Member lithologies in Toadstool Park. At Flagstaff Rim the transition from the Peanut Peak to the Big Cottonwood Creek lithologies occurs within a transitional zone that is between 20 and 70 meters from the base of the Flagstaff Rim measured section (Fig. 1.3).

1.3. Previous Work

Paleosols of the WRG have been extensively studied in Nebraska and South Dakota. Retallack (1983) conducted the first comprehensive study of paleosols within the WRG. His study analyzed 87 paleosols in the Dillon Pass/Pinnacles overlook area within Badlands National Park, SD (Fig. 1.1). Retallack (1983) calculated a decrease in mean annual precipitation (MAP) based on depth to Bk horizons from more than 1000 mm/yr in the late Eocene to 500-900 mm/yr in the early Oligocene. This trend was also noted in the Big Cottonwood Creek Member of the Chadron Formation by Terry (2001), who calculated a MAP decrease from 855 ± 282 to 739 ± 282 mm/yr leading up to the Eocene-Oligocene boundary at Toadstool Geologic Park, in northwest Nebraska (Fig 1.1). Sheldon and Retallack (2004) and Retallack (2007) calculated a decrease in MAP from 852 ± 156 to 628 ± 156 mm/yr in paleosols of western Nebraska. This change in precipitation is associated with an interpreted change in vegetation from forested landscapes in the late Eocene to a more open woodland and grassland of the early Oligocene (Retallack, 1983; Retallack, 1992; Terry, 2001; Strömberg, 2004). West to east changes in sediment have been noted by Evanoff et al. (1992), including changes from fluvial to fluvial plus eolian dominated processes in the late Chadronian at Flagstaff

Rim, WY to the Orellan at Toadstool Park, NE. Suggested changes in sediment are interpreted as a regional west to east climate gradient (Evanoff et al., 1992; Terry, 2001).

1.4. Stratigraphic Correlation

Previous tephrostratigraphic interpretations have suggested a correlation between Ash J at Flagstaff Rim, WY and the UPW of Schultz and Stout (1955) at Toadstool Park, NE (Fig. 1.4; Larson and Evanoff, 1998; Terry and LaGarry, 1998; Terry, 2001). Based on new zircon U/Pb dates (Sahy et al., 2010), this correlation is incorrect. The UPW is younger than the J Ash by approximately 300 ka. Regardless, these ashes provide a relative chronologic tie-point between these two regions just prior to the EOT and allow for regional comparisons of paleopedology at similar intervals of time. Below Ash J at Flagstaff Rim are 15 other ash beds, some of which have been dated using $^{40}\text{Ar}/^{39}\text{Ar}$ (Prothero, 1996; Sahy et al., 2010). Currently, there are no additional ash layers which can be unequivocally correlated from Flagstaff Rim to Toadstool Park. The age for the base of Flagstaff Rim was placed between 36 -36.5 Ma based on the presence of Chadronian fossils intermixed with late Duchesnean fossils (Prothero and Swisher, 1992). This age has been refined to 36.5-37 Ma, which is the current age for the Duchanian/Chadronian border (Prothero and Emry, 2004).

Chapter 2: Materials and Methods

2.1. Field and Microscope analysis

Paleosol profiles were excavated to expose fresh material. Grain size, Munsell® (2000) soil color, structure and horizon thickness of paleosols were recorded in the field. Measured sections reflect field observations only. Oriented hand samples were collected throughout individual profiles and prepared into a total of 84 thin sections for petrographic analysis following the methods of Brewer (1976), Retallack (1997), and Terry (2001).

2.2. Geochemical analysis

X-ray Diffraction (XRD) was used to analyze clay minerals and other secondary minerals such as calcite and quartz. A total of 53 oriented samples were analyzed on a Rigaku DMAX/B horizontal Diffractometer between 2-35° 2 θ using 35 kV and 15 mA CuK α radiation and a scan rate of 1.2°2 θ /min. Samples were prepared following the methods of Moore and Reynolds (1997) and analyzed in untreated and glycolated states.

Major, minor and trace elements in 41 samples were analyzed using X-ray Fluorescence spectrometry (XRF) at Franklin and Marshall College on a Panalytical 2404 XRF. Chemical compositions were used to calculate molecular weathering ratios. These ratios rely on the concept that paleosol weathering can be inferred based on certain molecular ratios of oxide compounds in modern soil environments (Table 2.1; Terry, 2001; Sheldon & Tabor, 2009). Molecular weathering ratios are dependent on water availability, because increased precipitation should lead to a soil with greater amounts of development (Birkland, 1999; Sheldon & Tabor, 2009). These ratios can therefore be used as clues to soil development and ultimately aide in the environmental interpretation

of the paleosol (Chesworth, 1992; Retallack, 1997). Clayeyness is a measure of clay formation and podzolization with numbers between 0.1 and 0.3 common for clay-rich soils and numbers near zero for sandy soils (Table 1; Retallack, 1997; Sheldon & Tabor, 2009). Calcification can be inferred based on the ratio of $(\text{CaO}+\text{MgO}/\text{Al}_2\text{O}_3)$. For alkaline soils the ratio is below 2, but up to 10 within carbonate nodules (Table 2.1; Retallack, 1997; Sheldon and Tabor, 2009). Soils with greater carbonate values and carbonate nodules likely formed in a more arid environment, whereas soils with little or no carbonate in similar parent materials likely formed in a more humid environment. The molar ratio of $(\text{Al}_2\text{O}_3/(\text{Al}_2\text{O}_3+\text{Na}_2\text{O}+\text{CaO}))$, referred to as CIA-K, as it compensates for burial metasomatism, can be used to infer paleoclimates based on Al_2O_3 being immobile and Na_2O and CaO being soluble (Sheldon and Tabor, 2009). The CIA-K values of subsurface B horizons can be used in paleoclimatic proxies to derive estimates of MAP (Table 2.1, 2). The total phosphate content within soils can give clues to the amount of organic matter accumulation and vegetation (Table 2.1; Smeck, 1973; Terry, 2001). The molar ratio of $\text{MgO}/\text{Al}_2\text{O}_3$ can be used as proxy to infer weathering of smectite, with an increase in the $\text{Mg}/\text{Al}_2\text{O}_3$ ratio with depth in the soil profile indicating the weathering of an overlying A horizon (Table 2.1). The molar ratio of bases/alumina $((\text{CaO}+\text{MgO}+\text{K}_2\text{O}+\text{Na}_2\text{O})/\text{Al}_2\text{O}_3)$, can be used to infer the pH of soils at time of formation, with ratios greater than unity suggesting alkaline/weakly developed soils and close to zero for strongly developed soils (Table 2.1). The ratio of Ba/Sr can be used to infer leaching, with acidic/well developed soils having ratios as high as 10 and most other soils having ratios around 2 (Table 1; Retallack, 1997).

Table 2.1: Molecular Weathering Ratios after Sheldon & Tabor (2009)

Molecular Weathering Ratios	Chemistry Form	Inferred Process
Clayeyness	(Al_2O_3/SiO_2)	podzilization
calcium/alumina	$(CaO + MgO/ Al_2O_3)$	calcification
CIA-K	$(Al_2O_3/(Al_2O_3+Na_2O+CaO))$	MAP proxy
magnesium/alumina	MgO/Al_2O_3	smectite weathering
total phosphorous content (oxide percent)	P_2O_5	organic matter
bases/alumina	$(CaO+MgO+K_2O+Na_2O)/Al_2O_3)$	Eluviations and illuviation
barium/strontium	Ba/Sr	leaching

Table 2.2: Paleoclimatic proxies after Sheldon and Tabor (2009)

Paleoclimate Proxy	Equation	r² value	Standard Error
MAP (mm/yr)	$P = 221.12e^{0.0197(CIA-K)}$	r ² =0.76	±182mm/yr
MAT-1 (°C)	$T = -18.5S + 17.3$	r ² =0.37	± 4.4 °C
MAT-2 (°C) (Inceptisol Specific)	$T = 46.9C + 4$	r ² =0.96	± 0.6 °C

CIA –K = Chemical Index of Alteration minus Potassium = (Al₂O₃/ (CaO+Na₂O+Al₂O₃))
S = Salinization = ((K₂O +Na₂O)/Al₂O₃)
C= Clayeyness = (Al₂O₃/SiO₂)

2.3. Classification

Ultisols, Alfisols, Aridisols, Inceptisols, Entisols and Mollisols have been previously documented within the White River Group (Retallack, 1983; Terry, 2001). All soils are classified based upon United States Department of Agriculture Soil Taxonomy (USDA Soil Survey Staff, 2010).

Chapter 3: Results

3.1. Paleosols

3.1.1. Tipps Trench Paleosol

Location: 42°48.785' N
106°43.465' W

Classification: Endoaqualf

Estimated Age: 36.6 ± 0.22 Ma

The Tipps Trench Paleosol is located 18 m above the base of Emry's (1973) measured section (Fig. 1. 3). The Tipps Trench Paleosol was named after its proximity to Tipps Oil Well and is located within the Peanut Peak Member equivalent lithology at Flagstaff Rim (Figs. 1.2a, d). The strata in this part of the section lack well-defined chronostratigraphic control due to the absence of volcanic ash beds. Biostratigraphy constrains the base of the Peanut Peak lithology to the earliest Chadronian at 37 Ma with Duchesnean taxa *Brachyhyops* and *Hemipsalodon* associated with earliest Chadronian fossils, similar to those of the Yoder beds of Wyoming (Prothero and Emry, 1996, 2004), which correlates to Chron C17.1n.

The A and Btg horizons of the Tipps Trench paleosol contain zones of olive green drab haloed root traces that trend downwards and horizontally (Fig. 3.1). In thin section, roots are preserved as both clay-lined root traces (Fig. 3. 2a) and as blocky diagenetic calcium carbonate void fill. Iron oxide mottles up to 1 mm in size are found throughout the A and Btg horizon (Fig. 3.2b). Strong skelsepic and lattisepic plasmic fabric and illuviated clays are common within the Btg horizon (Table 3.1). There is little evidence of calcification within this paleosol. The Tipps Trench paleosol is rich in smectite/illite clays with minor amounts of kaolinite (Fig 3.3).

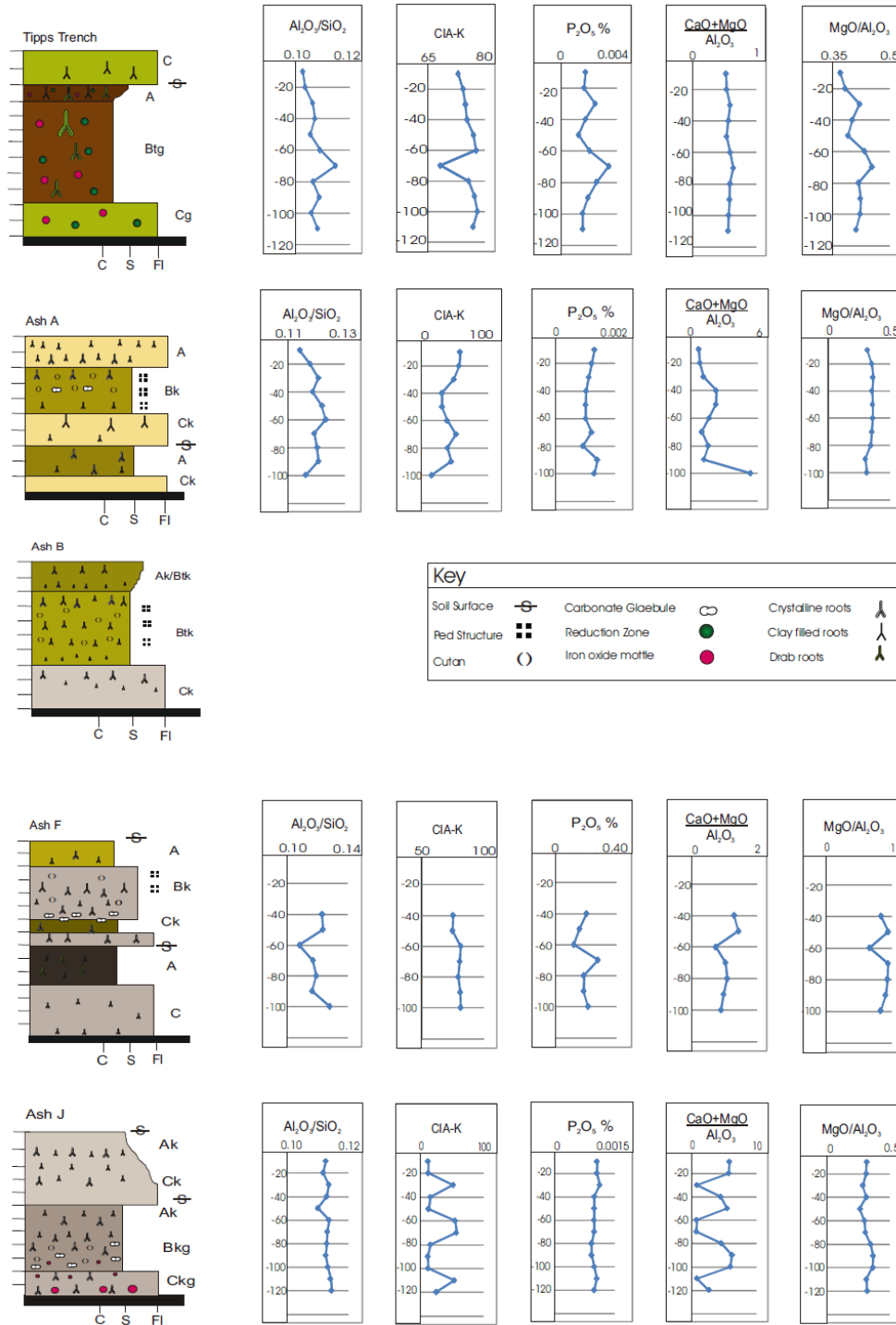


Figure 3.1. Measured section of individual soil profiles with graphs of selected geochemical trends vs. depth. Values are reported as the molar ratio of weight percentages of oxides. Chemical compositions were not analyzed from the Ash B paleosol.

The Tipps Trench paleosol is classified as an endoaqualf based on the presence of an argillic horizon. There is a gradual increase in clay with depth from the A to the Btg horizon. This same trend is noted in thin section as an increase in illuviated clay, as well as in the $\text{Al}_2\text{O}_3/\text{SiO}_2$ proxy, which suggests a pedogenic versus depositional origin (Fig 3.1). A slight decrease in the ratio of $\text{MgO}/\text{Al}_2\text{O}_3$ moving up section within this paleosol profile is interpreted as greater weathering of Mg rich smectite clays near the surface (Fig. 3.1). The P_2O_5 profile within this paleosol suggests a forested ecosystem where larger roots concentrate phosphorus deeper in the soil profile (Fig. 3.1; Hinkley et al., 1970; Smeck, 1973). The bases/alumina ratio suggests a slight decrease in bases from the A horizon, likely due to weathering, and gradual accumulation in the Btg horizon (Appendix I). The Ba/Sr ratio within this paleosol is inconclusive (Appendix I). Endoaqualfs are characterized by a fluctuating water table between the soil surface and base. Fluctuation of the water table at depth is inferred within the Tipps Trench paleosol by the presence of iron oxide mottles. The *endo* great group classification indicates that there is a lack of other diagnostic features.

Table 3.1: Description of the Tipps Trench Paleosol

0 to -20 cm	C horizon; sandstone, light greenish gray (10Y 7/1); sparse blocky calcite filled voids found sporadically throughout profile; fine grained quartz and feldspar sands dominate this horizon; skelsepic plasmic fabric; abrupt contact to...
- 20 to -30 cm	A Horizon; clay-rich sandstone, dark reddish brown (2.5YR 3/4); clay-filled and drab haloed root traces, hairline to 2 mm in diameter (10Y 7/1); illuviated clays and sparse root traces filled with calcite spar; roots 0.5-1 mm in diameter; sericite surrounds some quartz grains; quartz and feldspar have both a volcanic and plutonic origin as noted by the sweeping and undulatory extinctions within the quartz grains; smectite, inter-layered illite/smectite and illite are the dominant clay mineralogies with minor amounts of kaolinite; skelsepic with zones of lattisepic plasmic fabrics; gradual contact to...
-30 to -90 cm	Btg Horizon; mudstone, dark reddish brown (2.5 YR 3/4); clay filled root traces 0.1-0.5 mm in diameter and clay filled drab haloed root traces 0.5 – 4 mm in diameter; iron oxide mottles (10YR 2/1) up to 1 mm in diameter are abundant, as well as quartz grains surrounded by iron oxide rims; Tartan twined feldspars common; inter-layered illite/smectite and illite are dominant clay mineralogies, with minor amounts of kaolinite; kaolinite rims around mica grains; skelsepic to lattisepic plasmic fabric; abrupt contact to...
-90 to -110 cm	Cg Horizon; sandstone, light greenish grayish (10Y 7/1); iron oxide mottles (10YR 2/1) up to 1 mm in diameter throughout profile; sparse blocky calcified void fills; skelsepic plasmic fabric.

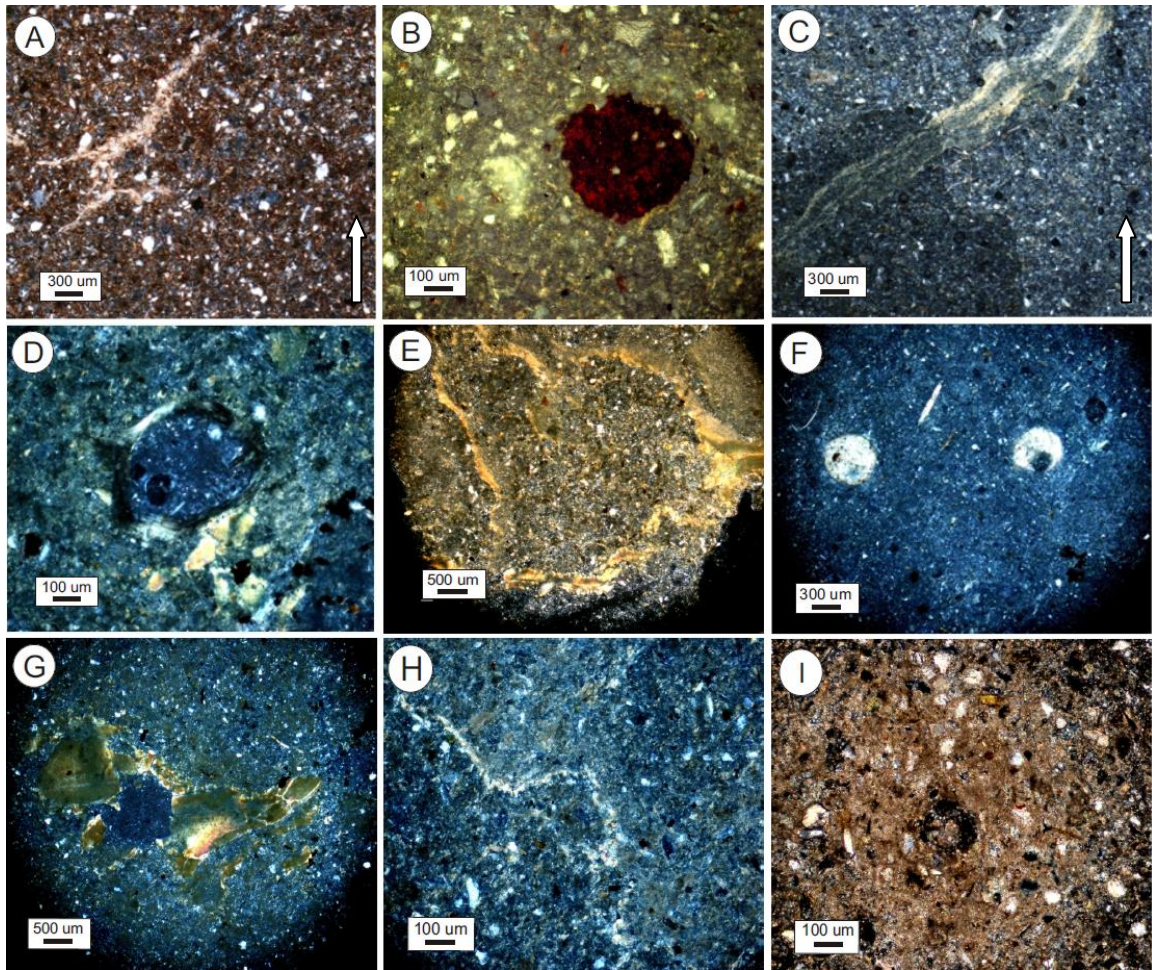


Figure 3.2. Photomicrographs of pedogenic features. All images are oriented horizontal to original horizons, unless otherwise denoted by an arrow, and photographed under cross polarized light. (A) Clay lined root trace from the Btg Horizon in Tipps Trench paleosol. (B) Iron oxide mottle from the Bkg horizon of Ash J under reflected light. (C) Clay filled root trace from the A horizon of Ash A paleosol. (D) Horizontal cross section through clay lined root trace within the Btk horizon of Ash B paleosol. (E) Clay lined ped from the Btk horizon of Ash B paleosol. (F) Two calcium carbonate glaeboles from the Bk horizon of Ash B paleosol. (G) Translocated clay from the Bk Horizon of Ash F paleosol. (H) Clay/calcite lined ped from the Bk horizon of Ash F paleosol. (I) A carbonate rhizolith from the Bkg horizon of the Ash J paleosol.

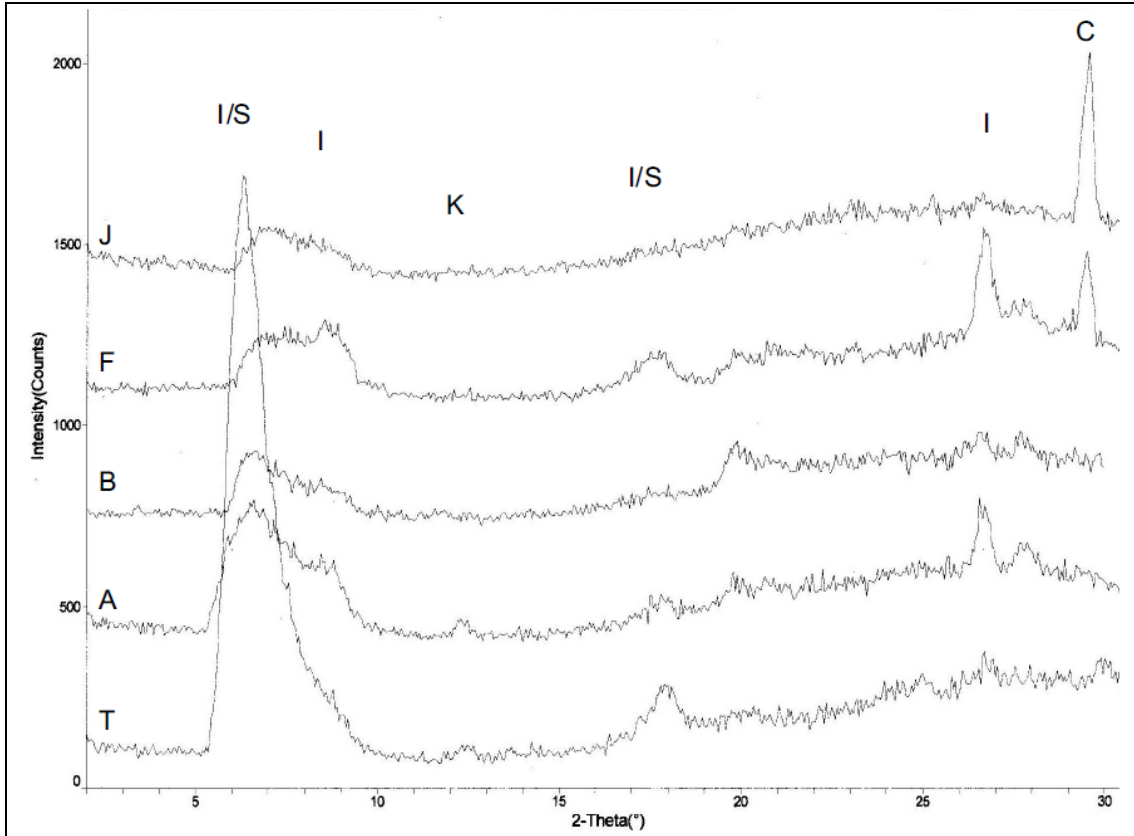


Figure 3.3. Untreated diffractograms from the B horizons of individual paleosol profiles. Note the decrease in smectite intensity and kaolinite intensity and the increase in calcite up section. T- Tipps Trench, A- Ash A, B- Ash B, F- Ash F, J – Ash J. I/S Interlayered Illite/Smectite, I – Illite, K – Kaolinite, I- Illite, and C- Calcite

3.2.2. Ash A Paleosol

Location: 42°38.176'N
106°44.491'W

Upper Paleosol Classification: Calciustept

Lower Paleosol Classification: Ustifluent

Estimated Age: 36.1 ± 0.22 Ma

The Ash A profile is located directly above Ash A, 47 m above the base of the WRG at Flagstaff Rim (Fig. 1. 2 b, 1.3). This ash does not correlate with any known tuffs within the WRG. The age of Ash A is determined by linear regression from Ash B and assumes a constant sedimentation rate between the base of the Flagstaff Rim section and Ash B. The Ash A paleosol is composed of two paleosols which have overprinted two fining-upward depositional packages (Fig. 3.1). Volcanic fragments are more prevalent within this paleosol package than in the Tipps Trench profile.

The upper paleosol has abundant clay-filled root traces up to 3 mm in diameter, blocky calcium carbonate fill, and rhizoliths up to 1 mm in diameter. Calcium carbonate glaeboles 1-2 mm in diameter have accumulated at depths greater than 40 cm in the paleosol profile. Clay-lined angular blocky peds are present within the A and Bk horizons of this profile. This is the oldest paleosol in this sequence to show rhizoliths, as well as calcium carbonate glaeboles. The upper Bk horizon of the upper paleosol contains zones of calcium carbonate accumulation of stage I-II, which increases to stage II in the lower Bk and C horizon (Table 3.2; Gile et al., 1966). Skelsepic plasmic fabric is common throughout the upper and lower paleosol profiles. Illite and interlayer smectite/illite are the dominant clay minerals with minor amounts of kaolinite and clay-sized calcite present (Fig. 3.3).

The lower paleosol contains sporadic clay-lined and carbonate spar-filled root traces ranging from 0.5-2 mm in diameter. The abundance of root traces decreases with depth; root traces are vertically oriented through this profile (Fig. 3.2c). Volcanic glass is more abundant in the lower paleosol than in the upper paleosol.

The upper paleosol of the Ash A profile is classified as a calciustep based on abundant rhizoliths and carbonate glaebules that suggest an ustic moisture regime. This paleosol overprints a crevasse splay deposit. There is a gradual accumulation of illuviated clays in the Bk horizon of the uppermost paleosol which is noted in thin section and by the “clayeyness” ratio through the profile (Fig. 3.1, 2c). Carbonate and clay lined root traces are prevalent in both the A and Bk horizon. There is a gradual increase in calcification with depth in the upper paleosol (Fig. 3.1). The calcification spike in the lower paleosol has been skewed by Ash A volcanic ash which is found at the base of the lower Ash A paleosol. There is a slight decrease in the ratio of MgO/Al_2O_3 moving up section within this profile indicating the weathering of smectite clays (Fig. 3.3). The P_2O_5 trend with depth is inconclusive for this paleosol. The bases/alumina ratio indicates a slight increase in bases with depth and is interpreted as the weathering and translocation of bases from the A horizon into the Bk horizon (Appendix I). There is a slight decrease in the Ba/Sr ratio within the upper paleosol which is interpreted as leaching of Sr from the A horizon (Appendix I). This paleosol is classified as an inceptisol based on the minor amount of soil development and the lack of diagnostic features that allow for further classification.

The lower paleosol is classified as an ustifluent. The presence of pedogenic carbonate indicates this soil formed in an ustic moisture regime. This soil has

overprinted a crevasse splay deposit indicating a fluvial origin of sediments. The greater abundance of volcanic glass, the sporadic clay-filled root traces and carbonate rhizoliths, and skelsepic clay fabric indicate little pedogenic development, which suggests this soil is an entisol.

Table 3.2: Description of Ash A Paleosol

0 to - 20 cm	A Horizon; sandstone, pale olive (5Y 6/3); clay-filled roots, 0.5 -3 mm in diameter, migrate vertically through horizon; carbonate rhizoliths 1 mm in diameter, filled with blocky calcite spar; angular to sub angular volcanic glass fragments; illite and interlayer smectite/illite with minor amounts of kaolinite and clay sized calcite; skelsepic plasmic fabric; abrupt contact to...
-20 to - 50 cm	Bk Horizon; siltstone, pale olive (5Y 6/4); clay and calcite spar filled roots 0.5-3 mm in diameter; rhizoliths 1-2 mm in diameter filled with blocky calcite spar infill; Stage I-II transitioning to Stage II carbonate glaeboles 1- 2 mm in diameter; illite and interlayer smectite/illite and clay sized calcite; skelsepic and insepic plasmic fabric; abrupt contact to...
-50 to -70 cm	Ck Horizon; sandstone pale olive (5Y 6/3); clay-lined and calcite spar filled root traces 0.5- 2 mm in diameter; stage II carbonate glaeboles 1- 2 mm in diameter ; smectite, illite and interlayer smectite/illite with minor amounts of kaolinite clays; skelsepic plasmic fabric; abrupt contact to...
-70 to -90 cm	A Horizon; siltstone olive (5Y 4/3); sparse clay filled root traces 0.5- 2 mm in diameter, diameter decreasing with depth; sporadic calcite spar filled root voids 0.5 mm in diameter; illite and interlayer smectite/illite with minor amounts of kaolinite and clay sized calcite; skelsepic plasmic fabric; abrupt contact to...
-90 to -100cm	Ck Horizon; sandstone pale olive (5Y 6/3); sparse clay filled root traces 0.5- 2 mm in diameter, decreasing with depth; sporadic calcite spar filled root voids 0.5 mm; stage II carbonate; pumice/volcanic fragments up to 0.5 mm in length; smectite, illite and interlayer smectite/illite clays dominant; skelsepic plasmic fabric.

3.1.3. Ash B paleosol

Location: 42°38.176'N
106°44.480'W

Classification: Haplustalf

Estimated Age: 35.99 ± 0.22 Ma

The Ash B paleosol is located 54 m from the base of the Flagstaff Rim section (Fig. 1.3). The trench for the Ash B paleosol is located 1.5 m below the base of Ash B, which is dated at 35.97 ± 0.22 Ma (Fig. 1.3). The top of this profile was not described due to the influence of modern day weathering. This paleosol was recognized in the field as a dark brownish/black band which pinched out laterally (Fig. 1.2e). The trench exposed the thickest extent of this band.

The Ash B paleosol is moderately to well-developed. The Ak/Btk horizon is rich in illuviated clays. The Btk horizon contains abundant downward-trending clay-lined and clay-filled roots and carbonate rhizoliths up to 1 mm in diameter (Fig. 3.2d). Subangular blocky clay-lined peds, 1 cm in diameter, are found within the Btk horizon of this paleosol (Fig. 3.2e). Stage II carbonate glaebules up to 2.5 mm in diameter are found in all horizons (Fig. 3.2f). Illite and interlayer smectite/illite are the dominant clay minerals (Fig. 3.3), with minimal amounts of smectite, kaolinite in the A horizon, and clay-sized calcite in the Btk horizon. Lattisepic and omnisepic plasmic clay fabrics dominate the Btk horizon of this soil (Table 3.3).

This paleosol is classified as a Haplustalf based on a significant amount of pedogenic carbonate, as evidenced by the rhizoliths and carbonate glaebules, which suggest that this paleosol formed within an ustic moisture regime. Illuviated clays, clay-

lined peds, ~ 1 mm in diameter, and abundant vertically oriented clay-lined root traces suggest the presence of an argillic horizon.

Table 3.3: Description of Ash B paleosol.

0 to -20 cm	Ak/Btk Horizon; top of paleosol profile truncated by modern weathering; sandy olive siltstone (5Y 4/3); clay and calcite filled root traces 1 mm in diameter; stage II carbonate glaebules up to 2.5 mm in diameter; clay lined sub angular blocky peds 1 cm in diameter; smectite, illite interlayered illite/smectite with minor amounts of kaolinite clay; skelsepic and weak lattisepic plasmic fabric, with gradual contact to...
-20 to -70 cm	Btk Horizon; siltstone pale olive to olive (5Y 6/3 transitioning to 5Y 4/3 at base); clay filled rhizoliths 1 mm in diameter; diagenetic calcium carbonate filled root traces 1-2 mm in diameter; clay lined root traces fine downwards from 1 mm in diameter to hairline; clay lined sub angular blocky peds 1 cm in diameter; illuviated clays and stage II carbonate glaebules ~ 2.5 mm in diameter; iron oxide rims around quartz grains; illite and interlayered illite/smectite clays are dominant with minor amounts of kaolinite; lattisepic and omnisepic plasmic fabric, with abrupt contact to...
-70 to -100 cm	Ck Horizon; sandstone light gray (5Y 7/2); large clay lined roots 4 mm in diameter; carbonate rhizoliths filled with calcite spar; stage II carbonate; skelsepic plasmic fabric.

3.1.4. Ash F Paleosol

Location: 42°38.787'N
106°45.547'W

Upper Paleosol Classification: Halpustept

Lower Paleosol Classification: Ustifluent

Estimated Age: 35.8 ± 0.04

Ash F is located 96 m from the base of the Flagstaff Rim section (Fig. 1.3) and correlates regionally with Ash 2 in Douglas, Wyoming (Fig. 1.4; Evanoff et al., 1992). The trench for the Ash F paleosol is located 1.5 m below the base of Ash F (Fig. 1.2c). The Ash F paleosol is composed of two separate paleosol profiles which have overprinted two fining-upward crevasse splay deposits (Fig. 3.1).

The uppermost A horizon was identified by isolated clay lined roots and carbonate rhizoliths 0.5-2 mm in diameter. The Bk horizon contains downward-trending clay lined roots and rhizoliths up to 1 mm in diameter. Stage II calcium carbonate glaebules up to 2.5 cm in diameter are present at the base of the Bk horizon (Fig. 3.2g). Small angular blocky peds within the Bk horizon are approximately 1 mm in diameter with clay and calcium carbonate cutans (Fig. 3.2h). The Ck horizon preserves some remnants of relict bedding as well as sparse calcite filled root traces ranging from hairline to 0.5 mm in diameter. Stage II carbonate accumulations are present within the Bk and Ck horizons, respectively. Poorly ordered illite/smectite and illite are common throughout the profile, with minor amounts of calcite in the Bk horizon (Fig. 3.3). Skelsepic plasmic fabric is the dominant clay fabric within the upper A horizon. Lattisepic plasmic fabric with zones of omniseptic plasmic fabric is found within the Bk horizon (Table 3.4).

The A horizon of the lower paleosol consists of mudstone that still preserves remnants of relict bedding and is overprinted by 1-2 mm diameter clay-filled drab-haloes root traces and sparse 1 mm diameter carbonate rhizoliths. The lower C horizon contains sparse hairline, clay-filled root traces.

The upper paleosol is classified as a haplustept. This paleosol contains rhizoliths and carbonate glaebules, which suggest the soil formed within the ustic moisture regime. The weak to moderate development of this paleosol, which is suggested by the roots, pedes and illuviated clays, indicate enough soil development to classify a Bk horizon. An increase in calcification within the Bk horizon of this paleosol is noted based on the $((\text{CaO}+\text{MgO})/\text{Al}_2\text{O}_3)$ profile (Fig. 3.1). There is a slight decrease in the ratio of $\text{MgO}/\text{Al}_2\text{O}_3$ moving up section within both paleosols. The P_2O_5 trend for the upper paleosol is not conclusive (Fig. 3.1). Bases/alumina trends throughout the upper paleosol are not conclusive due to a lack of geochemical data. The Ck horizon of the lower paleosol shows an increase in bases with depth and is interpreted as weathering and translocation of bases from the A horizon. Ba/Sr trends in the upper paleosol are inconclusive. This paleosol is weak to moderately developed and is classified as an inceptisol due to a lack of diagnostic features that would allow for other classification.

The lowermost paleosol is classified as an ustifluent. The presence of carbonate rhizoliths which overprint relict bedding indicates an ustic moisture regime and a fluvial origin of sediments, respectively. The presence of preserved relict bedding also suggests little soil development, which supports the classification of this soil as an entisol.

Table 3.4: Description of Ash F Paleosol

0 to -20 cm	A Horizon; mudstone, pale yellow (5Y 8/2); clay and calcite filled root traces hairline to 2 mm in diameter; roots migrate downward; carbonate rhizoliths 1 mm in diameter common; root voids filled with calcite spar 0.5-2 mm in diameter; root diameter decreases with depth; illuviated clays; interlayered illite/smectite and illite are dominant clays; skelsepic clay fabric, with abrupt contact to...
-20 to -60 cm	Bk Horizon; sandstone olive (5Y 4/2); clay and diagenetic calcite spar filled root traces 1 mm in diameter; rhizoliths with blocky calcium carbonate infill; small clay and calcium carbonate lined peds 0.5 mm in diameter; Stage II carbonate glaebules 25 mm in diameter at base of horizon; illuviated clay; interlayered illite/smectite, and illite with clay size calcite; insepic and skelsepic plasmic fabric, with abrupt contact to...
-60 to -80 cm	Ck; mudstone, dark olive gray (5Y 3/2) coarsening downward to sandstone light gray (5Y 7/2); root traces hairline to 0.5 mm in diameter filled with calcite spar; Stage II carbonate glaebules 25 mm in diameter at top of horizon ; relict bedding preserved in mudstone; interlayered illite/smectite and illite clays; skelsepic plasmic fabric; with abrupt contact to...
-80 to -110 cm	A Horizon; mudstone, dark olive gray (5Y 3/2); clay filled drab haloed root traces 1-2 mm in diameter; sporadic carbonate rhizoliths 1 mm in diameter; remnants of relict bedding preserved in mudstone; interlayered illite/smectite and illite clays; skelsepic plasmic fabric with abrupt contact to...
-110 to -150 cm	C Horizon; sandstone, pale yellow (5Y 7/2); sparse hairline clay filled root traces; interlayered illite/smectite and illite clays; skelsepic plasmic fabric.

3.1.5. Ash J Paleosol

Location: 42°38.496'N
106°45.826'W

Upper Paleosol Classification: Ustifluent

Lower Paleosol Classification: Aquic Calciustept

Estimated Age: 34.72 ± 0.03 Ma

Ash J is the uppermost ash within the WRG at Flagstaff Rim (Fig. 1.2c, f). The ash is located 213 m from the base of the section and is 6 m below the Miocene Split Rock Formation (Fig. 1.3). Ash J was thought to correlate with the 3c tuff in Douglas, WY and the Upper Purplish White layer (UPW) at Toadstool Park, NE (Fig. 1.4; Evanoff et al., 1992; Terry, 2001), but based on new zircon U/Pb dates (Sahy et al., 2010), this correlation is incorrect. The UPW is younger than the J Ash by approximately 300 ka.

The Ash J profile, located 0.5 m below Ash J, is composed of two fining-upward crevasse splay deposits which have been pedogenically overprinted by two separate paleosols (Fig. 3.1). The A horizon of the uppermost paleosol contains sparse 0.5 to 2 mm clay and carbonate-filled root traces. The C horizon of the uppermost paleosol contains subhedral to euhedral biotite and volcanic glass. The A and C horizons both contain Stage I-II carbonate (Table 3.5).

The lowermost paleosol is of greater importance in this study because it has more pedogenic development than the overlying paleosol. The lowermost A horizon contains clay and calcium carbonate filled root traces 1 mm in diameter. Carbonate rhizoliths up to 1 mm in diameter are present within this horizon (Fig. 3.2i). The underlying Bkg horizon contains illuviated clays, calcite-filled roots, and sparse rhizoliths running laterally

through the horizon with root diameters ranging from hairline to 1 mm in diameter. Iron oxide mottles, with diameters ranging from 0.5 to 1 mm, and stage II carbonate glaebules, up to 1 mm in diameter, are common within the Bkg horizon (Fig 3b, f). The Ckg horizon contains hairline calcium carbonate-filled root traces and iron oxide mottles 1 mm in diameter. Subhedral to euhedral zircons and biotite grains are common within this horizon. Stage I-II carbonate accumulations are present throughout all horizons (Table 3.5). This paleosol is characterized by illite and smectite clays with weak crystalline structure and clay sized calcite within the Bkg horizon of this paleosol (Fig. 3.3).

The uppermost paleosol is classified as an ustifluent. The presence of carbonate rhizoliths suggests an ustic moisture regime. This paleosol has overprinted a crevasse splay deposit, indicating a fluvial origin of sediments. It has been classified as an entisol based on the minor amount of soil development as indicated by sparse root traces, subhedral to euhedral volcanic fragments, and poorly ordered clay minerals.

The lower paleosol is classified as an aquic calciustept based on a combination of iron oxide mottles, carbonate rhizoliths, and stage II carbonate glaebules. The presence of iron oxides suggests this paleosol was subject to redoximorphic conditions, which places this soil in the *aquic* subgroup. The presence of rhizoliths and carbonate glaebules suggests this paleosol formed within an ustic moisture regime and places this soil in the *calci* great group. The weak to moderate development and the lack of diagnostic features restrict this soil to an inceptisol. Calcification increases within the upper Ck horizon and the lower Bkg and Ckg horizon (Fig. 3.1). As noted with previous soils, there is a decrease in the amount of MgO/Al_2O_3 moving up section within the lower paleosol indicating the leaching of Mg-rich smectite clays (Fig. 3.1). The P_2O_5 trend within the

Ash J profile is inconclusive (Fig. 3.1). There is an increase in the bases/alumina ratio with depth in the lowermost paleosol, which reflects the weathering and translocation of bases from the Ak horizon into the Bkg horizon (Appendix I). A decrease in the Ba/Sr ratio in this paleosol profile is thought to reflect leaching of Sr from the surface Ak horizon (Appendix I).

Table 3.5: Description of Ash J Paleosol

0 to -30 cm	Ak Horizon; siltstone, olive (5Y 6/3); sparse clay and micritic calcium carbonate root traces 0.5 – 2 mm in diameter; stage I-II calcium carbonate; sporadic illuviated clays; interlayered illite/smectite and illite; skelsepic plasmic fabric; with gradual contact to...
-30 to -50 cm	Ck Horizon; siltstone, pale olive (5Y 6/3) coarsening downward into sandstone (5Y 6/3); stage I-II calcium carbonate; abundant volcanic glass and pumice fragments; euhedral and subhedral biotite grains; iron oxide rims coating quartz grains; interlayered illite/smectite and illite; weak skelsepic plasmic fabric; with abrupt contact to...
-50 to -70 cm	Ak Horizon; siltstone, light gray (5Y 7/2); clay and calcium carbonate filled root traces 1 mm in diameter; carbonate rhizoliths 1 mm in diameter filled with calcite spar; stage I-II carbonate; iron-oxide rims surrounding quartz grains; interlayered illite/smectite and illite clays; skelsepic plasmic fabric; with abrupt contact to...
-70 to -100 cm	Bkg Horizon; siltstone, light gray (5Y 6/3); abundant calcite and clay filled root traces hairline - 1 mm in diameter; carbonate rhizoliths filled with calcite spar; stage II carbonate glaebules 1 mm in diameter; iron oxide mottles (10YR 2/1) ranging from 0.5 to 1 mm in diameter; interlayered illite/smectite, illite and clay size calcite dominant; skelsepic and weak lattisepic plasmic fabrics; with abrupt contact to...
-100 to -120 cm	Ckg Horizon; sandstone, pale olive (5Y 6/3); hairline calcium carbonate-filled root traces; stage I-II calcium carbonate; volcanic fragments abundant; subhedral zircons and biotite grains common; iron oxide mottles (10YR 2/1) 1 mm in diameter; interlayered illite/smectite and illite clays; skelsepic plasmic fabric.

Chapter 4: Discussion

4.1 Soil Formation

4.1.1. Climate

The transition from the variegated red and green clay-rich sediments within the Peanut Peak lithology at the base of the section to the overlying dark brown silt/claytone and yellowish sandstone of the Big Cottonwood Creek lithology suggests a gradual change in precipitation, similar to interpretations from the Chadron Formation of northwest, NE (Terry, 1998; 2001). Thin section and geochemical evidence both support this interpretation. The Tipps Trench paleosol has greater amounts of weathering and oxidation, is rich in smectite clays, with some kaolinite, and lacks pedogenic carbonate. The sediments between Ash A and Ash J are not as weathered and suggest drier conditions or increased seasonality. The 001 kaolinite peak is present in XRD patterns from the Tipps Trench, Ash A, and Ash B paleosols, whereas no kaolinite is identified within Ash F and J paleosols, but calcite is present (Fig. 3.3). Pedogenic carbonate is present in Ash A through Ash J paleosols, with the depth to carbonate similar in all profiles. The absence of pedogenic carbonate in the Tipps Trench paleosol can be explained by greater precipitation. Carbonate is readily dissolved, and during times of increased precipitation, pedogenic carbonate will be absent from soil profiles. If the climate becomes drier, the amount of pedogenic carbonate within the soils should increase (Birkeland, 1999), which is supported by macroscopic and morphological observations. In North America, the carbonate isohyet is 760 mm/yr, with carbonate absent from profiles receiving over 760 mm/yr (Retallack, 2005). Pedogenic carbonate is

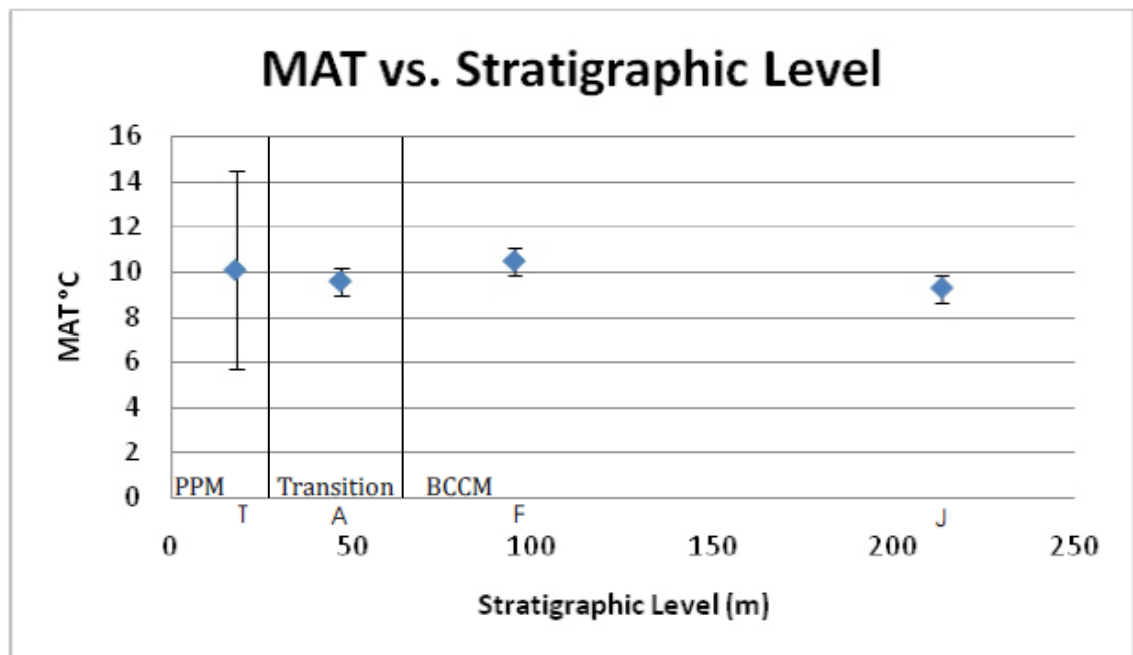


Figure 4.1. Graphs of the variations in MAP and MAT in paleosols calculated from climofunctions of Sheldon and Tabor (2009), and related to changes in sedimentology as indicated by the the Peanut Peak (PPM), transitional zone, and Big Cottonwood Creek (BCCM) lithologies. The Tipps Trench paleosol mean annual temperature calculated using MAT-1. The Ash B, Ash F and Ash J paleosols mean annual temperature calculated using MAT-2, which is inceptisol specific. MAT-1 yields similar results for Ash B, Ash F and Ash J paleosols (Appendix 1).

present in all paleosols above the Tipps Trench paleosol, suggesting precipitation was less than 760 mm/yr for all overlying paleosols in this study (Fig. 4.1).

The paleosols at Flagstaff Rim record a change from humid to semi-arid conditions over a 2.5 Ma period. The evidence at Flagstaff Rim suggests that the transition from humid to semi-arid conditions took place in as little as 800,000 years. A decrease in paleoprecipitation rates from 942 ± 182 mm/yr to 469 ± 182 mm/yr between the Tipps Trench and Ash A paleosols has been calculated based upon climofunctions (Fig. 4.1). The greatest decrease in paleoprecipitation rates takes place between the Tipps Trench and Ash J paleosols, where climofunctions suggest a change from 942 ± 182 mm/yr to 301 ± 182 mm/yr (Fig. 4.1; Appendix I). This finding is similar that of Zanazzi (2008), who found an increase in $\delta^{13}\text{C}$ values in fossil tooth enamel at Flagstaff Rim from $-9.08 \pm 0.06\text{‰}$ to $-8.54 \pm 0.10\text{‰}$, indicating a possible increase in water stress at $\sim 35.4\text{Ma}$. There is no significant change in MAT at Flagstaff Rim. Temperature fluctuates up section between 10.1 ± 4.4 °C for the Tipps Trench paleosol to 9.3 ± 0.6 °C for the Ash J paleosol based upon climofuntions (Fig. 4.1; Table 2; Appendix I).

4.1.2. *Organisms*

Roots are the most common trace fossils found within the paleosol profiles at Flagstaff Rim. The roots in the Tipps Trench paleosol are easily recognized as drab halo and clay-filled root traces. These roots tend to be relatively larger, up to 4 mm in diameter and can be seen without the use of a hand lens. Higher in the section, near Ashes F and J, roots tend to be smaller, with the largest roots up to 2 mm in diameter with calcium carbonate and clay films being the common modes of preservation. The change from more robust root traces, up to 4 mm in diameter, to smaller, more hairline root traces, suggests a change in vegetation.

Tipps Trench has been classified as an endoaqualf, which suggests that it harbored a forest-like environment (USDA Soil Survey Staff, 2010; Terry 2001). P_2O_5 accumulated lower in the Tipps Trench paleosol profile, which is suggestive of forested ecosystems where larger roots can translocate phosphate deeper in soil profiles (Hinkley et al., 1970; Smeck, 1973). The paleosols above Tipps Trench have fine root traces and abundant carbonate, and have been classified as both inceptisols and alfisols within an ustic moisture regime; both are common soils in modern savanna/grassland ecosystems. P_2O_5 trends for Ash A through J paleosol are not conclusive, although there is a slight enrichment within the lower A horizon of the Ash F paleosol. Aside from roots, worm fecal pellets have been found within Ash I, suggesting bioturbation. A large invertebrate burrow, 2.5 cm in diameter, was found between Ashes F and G.

4.1.3. Relief

Surface topography varied up to 120 m at Flagstaff Rim at the beginning of deposition (Emry, 1973). Sediment transport at this time was dominated by fluvial activity with sediment deposition occurring within the valleys. As the valleys filled, and fluvial plus eolian deposition increased with the influence of volcanics from the Great Basin, the topographic variation at Flagstaff Rim decreased (Emry, 1973). The general transition from fluvial to fluvial plus eolian deposition occurs between the Peanut Peak Member lithology and the Big Cottonwood Creek Member lithology within a transitional zone. The variations in topography at the lower stratigraphic levels are evidence of paleocatenas. Paleosols affected by paleocatenary relationships would have a lower MAP due to a greater concentration of bases, suggesting the inferred MAP of Tipps Trench paleosol is the minimum MAP (Table 1, 2). Variations in topography become minimal above the Peanut Peak lithology and therefore have little influence on all paleosols above Tipps Trench. These catenas can be identified in some cases by the ashes, which mantle them. They can also be recognized as overbank mudstones which taper in all directions.

All paleosols in this study, with the exception of Ash B, formed on flood plains where they were subject to burial by overbank floods. This is inferred by the presence of hydromorphic features and/or pedogenic overprinting of crevasse splay deposits. The Tipps Trench and Ash J paleosols contain iron oxide mottles, which indicate hydromorphy. The Ash A, F and J paleosols are thin, none exceeding 1 m in thickness, and overprint crevasse splay deposits, which suggest pedogenesis occurred on a floodplain with periodic overbank floods. Ash B is a well drained soil with vertically

trending root traces lined by both clay and calcite. This soil formed within a paleodepression that was slowly filled, which can be recognized in the field as a dark band that tapers on either side of the Ash B trench (Fig 1.2e).

4.1.4. Parent Material

The WRG is recognized as a volcanoclastic sequence composed of fine grained sandstone, siltstone and mudstone, with central Colorado, the Basin and Range of Nevada and western Utah, and local Laramide uplift providing the main source for the sediments (Evanoff et al., 1992; Larson and Evanoff, 1998). The sediments within the Peanut Peak lithology of the Tipps Trench paleosol contain dark red oxidized clay rich mudstone overlain by reduced greenish/gray silty sandstone. All paleosols contain smectite, indicating weathered volcanic ash as parent material. The decrease in the amount of smectite upsection is thought to indicate a change in weathering intensity and not parent material, as volcanic fragments are present in all thin sections and similar $\text{TiO}_2/\text{Al}_2\text{O}_3$ ratios exist in each paleosol (Fig. 4.2; Sheldon and Tabor, 2009). The sediments within the Big Cottonwood Creek lithology become enriched with volcanic ash, pumice fragments, euhedral biotite, and zircons identified within C horizons suggesting a change from a fluvial dominated to fluvial and eolian dominated system. This trend from fluvial to fluvial plus eolian deposition is thought to occur around Ash I at Flagstaff Rim (Evanoff et al., 1992) but may have begun as early as Ash B, which corresponds to increased volcanism from the Great Basin, as well as a sedimentation rate increase from 51 to 300 mm/Kyr (Fig. 4.3).

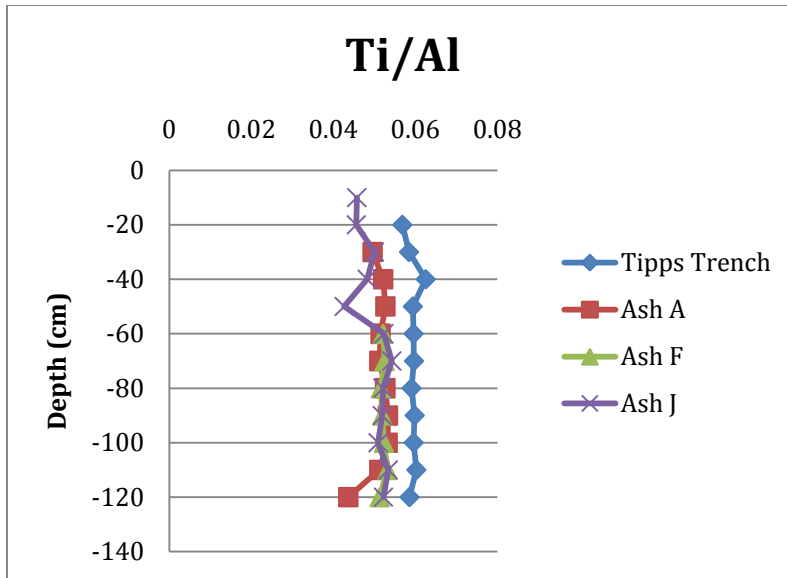


Figure 4.2. Graph of Ti/Al trend suggesting a shared provenance for all samples. Slight separation between Tipps Trench profile and overlying profiles may reflect an increase in volcanic ash due to an increase in volcanism which occurred after the formation of the Tipps Trench paleosol (Larson and Evanoff, 1998)

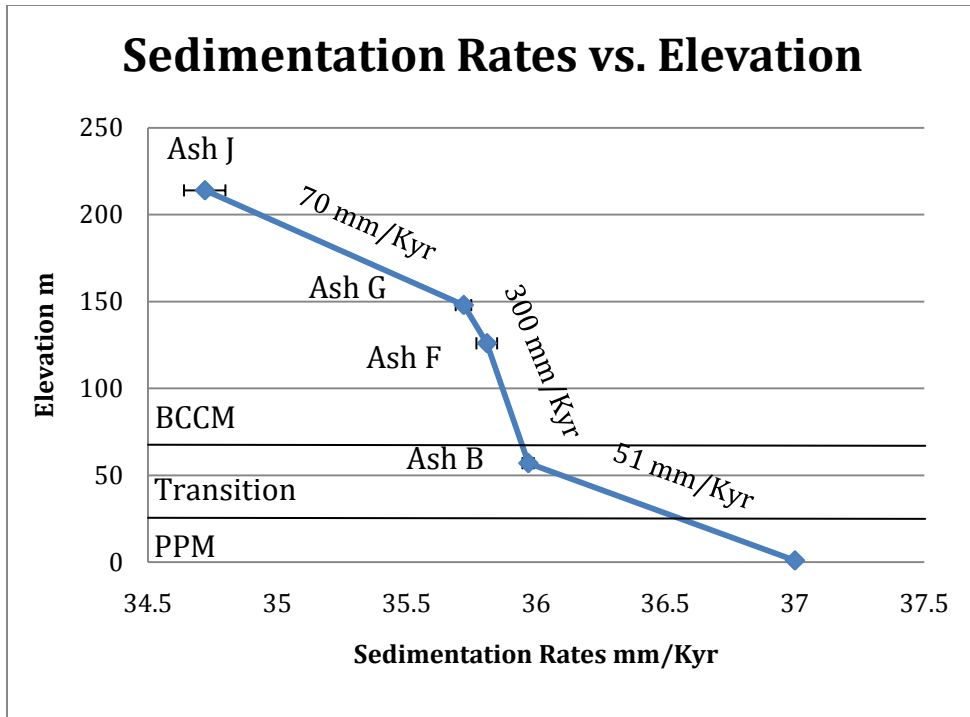


Figure 4.3. Sedimentation rates at Flagstaff Rim, WY versus lithology. Rates calculated using $^{40}\text{Ar}/^{39}\text{Ar}$ dates from Prothero and Swisher (1992) with associated errors and outcrop thickness from (Emry, 1973). The contact between the Peanut Peak (PPM), transitional, and Big Cottonwood Creek lithologies (BCCM) is denoted by two lines.

4.1.5. Time

The majority of sediments at Flagstaff Rim represent fluvial overbank flood plus eolian deposits 0.5-1 m in total thickness. Sedimentation rates are averaged to 51 mm/Kyr for soils formed between Tipps Trench and Ash B, and assuming rapid deposition of 0.5-1 m of overbank flood sediment, paleosols in this part of the section formed within 10,000-20,000 years. The Ash F paleosol formed during the period of highest sedimentation, and assuming rapid sedimentation, each 0.5-1 m paleosol formed within 1,400 - 3,100 years. The Ash J paleosol formed during a period of lower sedimentation rates, and assuming rapid sedimentation in packages of 0.5-1 m thick, the paleosols formed between 7,000-14,000 years.

The soil order and degree of calcification also give clues to the time allotted for soil formation (Gile et al., 1966; Retallack, 1997). Alfisols and inceptisols have both been identified in this study. In general, argillic horizons need a minimum of 10,000 years to form, suggesting that the Tipps Trench and Ash B paleosols are the most mature paleosols in this study (Birkeland, 1984). The maturity of the Tipps Trench and Ash B paleosols is also supported by the low sedimentation rates, with more mature paleosols being associated with lowest sedimentation rates. Ash A, F and J paleosols have zones of stage I- II carbonate accumulation, which are thought to take a minimum of 8,000 to 15,000 years to form (Gile et al., 1966). The paleosols above Ash B formed during the highest sedimentation rates, which likely contribute to the more weakly developed paleosols.

4.2. Sedimentation Rates vs. Climate

The Tipps Trench and Ash B paleosols formed over a similar amount of time based on sedimentation rates and soil type, yet these two paleosols differ drastically in morphology and clay mineralogy, suggesting precipitation as a limiting factor in soil formation. Based on paleosol morphology, an increase in aridity/seasonality appears to have occurred after the formation of the Tipps Trench paleosol and before the formation of Ash A paleosol. This trend is reflected in all paleosols above the Tipps Trench paleosol at Flagstaff Rim, as noted by the increase in pedogenic carbonate, a decrease in the illite/smectite peaks, and the disappearance of kaolinite. Paleosols formed after the Tipps Trench paleosol are less developed likely due to a decrease in MAP, increase in seasonality, or sedimentation rate. The presence of illuviated clays and iron oxide mottles overprinted by pedogenic carbonate indicate that paleosols at Flagstaff Rim experienced alternating wet and dry conditions ~36 Ma.

4.3. Regional Variations

Terry (2001) identified the transition from the Peanut Peak Member to the Big Cottonwood Creek member within Chron C16.1n at Toadstool Park, NE, based on the data presented by Prothero (1996). At Flagstaff Rim this transition takes place at the base of Chron C16.1n based on Prothero (2004). Dates from Prothero and Swisher (1992) compared to the astronomical time scale of Palike et al. (2006) suggest the transition between the Peanut Peak and Big Cottonwood Creek Member occurred within Chron 16.2n. Further evidence of regional differences arise with the comparison of the Darton pedotype of Toadstool Park, NE from Terry (2001) to the Ash J paleosol. The Darton pedotype is located directly below the UPW and has an interpreted MAP of 862 ± 182 mm/yr (Terry, 2001). This drastically differs from the Ash J soil with a MAP of 301 ± 182 mm/yr (Appendix I). A difference in mean annual precipitation between Flagstaff Rim and Toadstool Park, NE is evident despite a decrease in elevation of over 500 m from Wyoming to Nebraska. The amount of precipitation should increase with elevation (Daly et al. 1994). This difference in elevation, while it does not explain precipitation differences, may help explain the drop in $\delta^{18}\text{O}$ across the Eocene/Oligocene Boundary in northwest Nebraska reported by Zanazzi et al. (2007; 2009). Fossil teeth and bone from Chadronian age mammals came from Eastern Wyoming and Nebraska while fossil teeth and bone from Orellan/Whitneyan age mammals came from South Dakota and Nebraska (Fig. 4.4). $\delta^{18}\text{O}$ of fossil tooth enamel and bones reflect local rainwater composition (Kohn and Law, 2006). Meteoric water should therefore be isotopically lighter in Wyoming which may explain the observed shift in $\delta^{18}\text{O}$ up-section (Fig. 4.4; Sheppard et al., 1969).

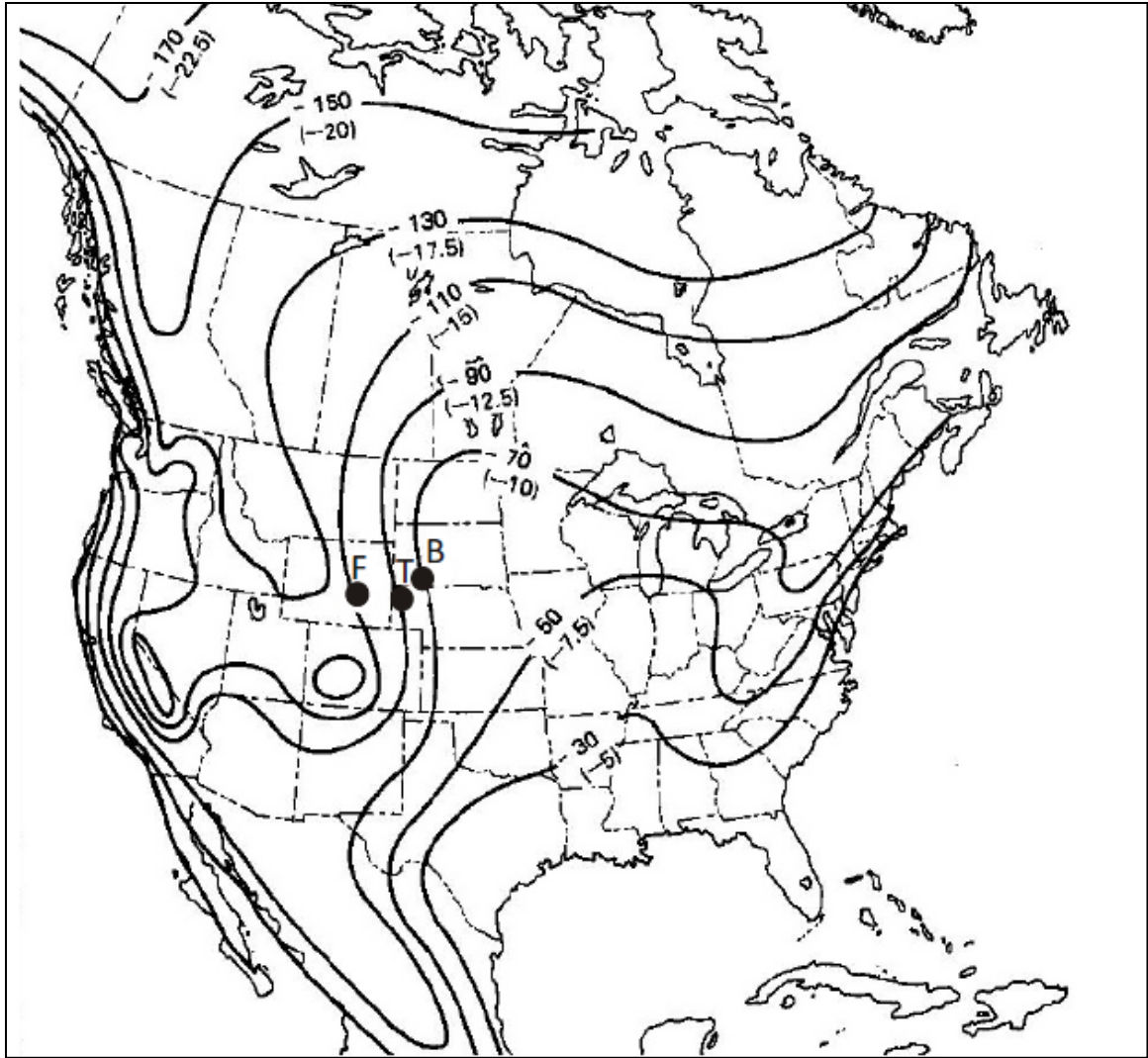


Figure 4.4. Current $\delta^{18}\text{O}$ variations of rain water in the United States and Canada modified from Sheppard et al. (1969), $\delta^{18}\text{O}$ isotopes are reported in parentheses. Dots are approximate locations of Flagstaff Rim, WY (F), Toadstool Park, NE (T), and Badlands National Park, SD (B).

The aridification at Flagstaff Rim, WY occurs prior to the Oi-1 event (33.65 Ma), suggesting an alternate cause of cooling. The building of partial or ephemeral Antarctic ice sheets occurs ~37 Ma, which eventually gave way to the Oi-1 event and permanent ice sheets at 33.65 Ma (Zachos et al., 2001). Although full glaciation does not occur until the Oligocene, the building of ephemeral ice sheets on Antarctica may have contributed to the increase in aridity at Flagstaff Rim. Increased volcanism (36 Ma) and impact events (36-35.5 Ma) correspond with the transitional zone between the Peanut Peak and Big Cottonwood Creek lithologies at Flagstaff Rim, as well as with the decrease in MAP from the Tipps Trench paleosol to the Ash A paleosol. Although volcanism and impacts are synchronous with the suggested increase in seasonality/aridity, it is unlikely that either can explain the long-term climatic perturbation that persists (Prothero, 1992). Volcanism and impact scenarios may instead have only compounded the effects of ephemeral ice sheets and the orographic effects of the Rocky Mountains, which have a large influence on local climates (Whitlock and Bartlein, 1993).

Local variations in orography and the establishment of the Oi-1 have both been used to explain regional differences in precipitation leading up to the EOT (Sheldon et al., 2009). Nebraska does not show permanent signs of drying until much later in the Oligocene, suggesting the Oi-1 had a greater effect than orography; however, the difference in paleosol development and MAP between Flagstaff Rim and Toadstool Park 644 km to the east of Flagstaff Rim is likely an orographic effect. Flagstaff Rim, WY had a MAP of 301 ± 182 mm/yr in the late Eocene, which is similar to the modern day average of 330 mm/yr (NOAA Website). This similarity suggests that the rain shadow effect caused by the Rocky Mountains became prominent within the late Eocene.

Chapter 5: Conclusions

The transition from the “hummocky” Peanut Peak lithology to the more resistant “cliff forming” Big Cottonwood Creek lithology occurs gradually within a transitional zone at Flagstaff Rim and is likely explained by a decrease in precipitation compounded by an increase in sedimentation rates. The paleosols at Flagstaff Rim, WY suggest an increase in aridity up section. This change is noted in paleosol geochemistry, macro- and micromorphology, and clay mineralogy. There is an increase in pedogenic carbonate and a decrease in smectite and kaolinite in profiles from the base to the top of the section. The Tipps Trench and Ash A paleosols formed during a period of similar sedimentation rate yet the morphology between these paleosols differ. The Tipps Trench paleosol is smectite-rich, shows evidence of oxidation and no pedogenic carbonate. The Ash A paleosol is smectite poor and shows an increase in volcanic fragments and pedogenic carbonate. The difference between the Tipps Trench and the Ash A paleosol morphology can be explained by a decrease in MAP rather than an increase in sedimentation rate. The Ash A paleosol and all overlying paleosols have a similar morphology, with a decrease in clay crystallinity and an increase in pedogenic carbonate. While it is likely that the decrease in precipitation is the limiting factor for paleosol morphology between the Tipps Trench and Ash A paleosols, an increase in sedimentation may have contributed to the decrease in paleosol morphology for paleosols which formed above Ash B. The Ash F and J paleosols were formed during a period of increased sedimentation, which corresponds with an increase in volcanism from the Great Basin. This increase in sedimentation likely compounded the effects of a decrease in MAP and can explain the weak paleosols development within the Big Cottonwood Creek lithology

at Flagstaff Rim. This agrees with the preliminary finding of Zanzazi (2008) of an increase in drying/seasonality occurring at ~35.4 Ma.

Sheldon et al., (2009) used regional orographic differences and the Oi-1 glaciation to explain variations in the late Eocene paleoclimatic record. Regional topographic differences between Flagstaff Rim, WY and Toadstool Park, NE likely explain differences in paleosol morphology between the two locations. Drying at Flagstaff Rim occurred prior to the Oi-1 event, suggesting that the building of ephemeral glaciers, combined with the rain shadow effect of Rocky Mountains, likely contributed to the late Eocene climate deterioration at Flagstaff Rim, WY. There is no discernable difference in temperature up section in the late Eocene at Flagstaff Rim based on paleosol evidence. Variations in temperature within the White River Group suggested by Zanzazi et al. (2007, 2009) are consistent with regional isotopic variations of meteoric water which, may explain observed shift in $\delta^{18}\text{O}$ isotopes.

REFERENCES

- Alvarez, W., Claeys, P., and Montanari, A., 2009, Time-scale construction and periodizing in Big History: From the Eocene-Oligocene boundary to all the past: Geological Society of America Special Paper 452, p. 249-259.
- Aubry, M-P., and Bord, D., 2009, Reshuffling the cards in the photic zone at the Eocene/Oligocene boundary: Geological Society of America Special Paper 452, p. 249-259.
- Birkeland, P.W., 1999, Soils and geomorphology, 3rd edition Oxford University Press, New York, NY, p. 203, 218-224, 290.
- Best, M.G., Christiansen, E.H., Deino, A.L., Gromme, C.S., McKee, E.H., and Nobel, D.C., 1989, Eocene through Miocene Volcanism in the Great Basin of the western United States: New Mexico Bureau of Mines and Mineral Resources Memoir 47, p. 91-133
- Bottomley, R., Grieve, R., York, D., and Masaitis, V., 1997, The age of the Popigai impact event and its relation to events at the Eocene/Oligocene boundary: Nature, v. 388, p. 365-368.
- Brewer, R., 1976, Fabric and mineral analysis of soils, 2ed edition Krieger, New York, NY, p. 482.
- Brown, R.E., Koeberl, C., Montanari, A., and Bice, D.M., 2009, Evidence for change in Milankovitch forcing caused by extraterrestrial events at Massignano, Italy, Eocene-Oligocene boundary, GSSP: Geological Society of America Special Paper 452, p. 119-137.
- Bryant, J.D., Froehlich, P.N., Showers, W.J., Genna, B.J., 1996, Biologic and climatic signals in the oxygen isotopic composition of Eocene-Oligocene equid enamel phosphate: Paleogeography, Paleoclimatology, Paleoecology, v. 126, p. 75-89.
- Chesworth, W., 1992, Weathering Systems, *in* Martini, I.P. and Chesworth, W., eds., Weathering soils and paleosols, Elsevier, Amsterdam, p. 19-40.
- Coccioni, R., Frontalini, F., and Spezzaferri, S., 2009, Late Eocene impact-induced climate and hydrological changes: Evidence from the Massignano global stratotype section and point (central Italy): Geological Society of America Special Paper 452, p. 249-259.
- Daly, C., Neilson, R.P., and Phillips, D.L., 1994, A statistical topographic model for mapping climatological precipitation over mountainous terrain: Journal of Applied Meteorology, v. 33, p. 140-158.

- Darton N.H., 1908, Paleozoic and Mesozoic of Central Wyoming: Bulletin of the Geological Society of America, 19:403-474, plates 21-30.
- Emry, R.J., 1973, Stratigraphy and preliminary biostratigraphy of the Flagstaff Rim area, Natrona County, Wyoming: Smithsonian Contributions to Paleobiology, v. 18, p.1-43.
- Evanoff, E., Prothero, D.R., Lander, R.H., 1992. Eocene–Oligocene climatic change in North America: the White River Formation near Douglas, east-central Wyoming, *in* Prothero, D.R., Berggren, W.A. eds., Eocene–Oligocene Climatic and Biotic Evolution, Princeton University Press, Princeton, NJ, p. 116– 130.
- Gile, L.H., Peterson, F.F. & Grossman, J.B., 1966, Morphological and genetic sequences of carbonate accumulation in desert soils: Soil Science, v. 101, p. 347-360.
- Hilgen, F.J., and Kuiper, K.F., 2009, A critical evaluation of the numerical age of the Eocene-Oligocene boundary: Geological Society of America Special Paper 452, p. 249-259.
- Hinkley, K.C., Runge, E.C.A., Pedersen, E.J., 1970, Effect of soil on vegetation in NE Illinois, Agronomy Abstracts, 137.
- Koeberl, C., 2009, Late Eocene impact craters and impactoclastic layers-An overview: Geological Society of America Special Paper 452, p. 249-259.
- Kohn, M.J., and Law, J. M., 2006, Stable isotope geochemistry of fossil bone as a new paleoclimate indicator: Geochimica et Cosmochimica Acta, v. 70, p. 931-946.
- Larson E.E., and Evanoff, E., 1998, Tephrostratigraphy and source of the tuffs of the White River Sequence: Geological Society of America Special paper 325, p. 1-14.
- McGowran, B., 1989, Silica burp in the Eocene ocean: Geology, v. 17, p. 857-860.
- McGowran, B., Moss, G., and Beecroft, A., 1992, Late Eocene and early Oligocene in southern Australia: Local neritic signals of global oceanic changes, *in* Prothero, D.R., Berggren, W.A. eds., Eocene–Oligocene Climatic and Biotic Evolution, Princeton University Press, Princeton, NJ, p. 116– 130.
- Miller, K.G., Berggren, W.A., Zhang, J., and Palmer-Julson, A.A., 1991, Biostratigraphy and isotope stratigraphy of the upper Eocene Microtektites at site 612: how many impacts?: Palaios, v. 6, p. 17-38.
- Miller, K.G., Wright, J.D., Katz, M.E., Wade, B.S., Browning, J.V., Cramer, B.S., and Rosenthal, Y., 2009, Climate threshold at the Eocene-Oligocene transition: Antarctic ice sheet influence on ocean circulation: Geological Society of America Special Paper 452, p. 249-259.

- Moore, D.M. and Reynolds, R.C., Jr., 1997, X-Ray Diffraction and the Identification and Analysis of Clay Minerals 2ed: Oxford University Press, New York, NY, p. 378.
- Munsell, 2000, Munsell Soil Color Chart: GretagMacbeth, New Windsor, NY.
- Palike, H., Norris, R.D., Herrle, J.O., Wilson, P.A., Coxall, H.K., Lear, C.H., Shackleton, N.J., Tripathi, A.K., and Wade, B.S., 2006, The Heartbeat of the Oligocene climate system: *Science*, v. 314, p. 1894-1898.
- Poag, C.W., Koeberl, C., and Reimold, W.U., 2004, The Chesapeake Bay crater- geology and geophysics of the late Eocene submarine impact structure: Heidelberg, Germany, Springer, p. 522.
- Premoli Silva, I., and Jenkins, D.G., 1993, Decision on the Eocene-Oligocene boundary stratotype: *Episodes*, v. 16, p. 379-382.
- Prothero, D.R., 1992, Glacier, Volcanoes, or Asteroids, *in* Prothero, D.R., Berggren, W.A. (Eds.), *Eocene–Oligocene Climatic and Biotic Evolution*, Princeton University Press, Princeton, NJ., p. 224-246.
- Prothero, D.R., 1996, Magnetic Stratigraphy of the White River Group in the High Plains, *in* Prothero, D.R., and Emry R.J., eds., *The terrestrial Eocene- Oligocene transition in North America*: Cambridge, U.K., Cambridge University Press, p. 262-277.
- Prothero, D.R., 2004, Did impacts, volcanic eruptions, or climate change affect mammalian evolution?: *Paleogeography, Paleoclimatology, Paleoecology*, v. 214, p. 283-294.
- Prothero, D. R., and Emry, R., 1996, Summary, *in* Prothero, D.R., and Emry R.J., eds., *The terrestrial Eocene- Oligocene transition in North America*: Cambridge, U.K., Cambridge University Press, p. 664-683.
- Prothero, D. R., and Emry, R.J., 2004, The Chadronian, Orellan, and Whitneyan North American Land Mammal Ages, *in* Woodburne, M. O., eds., *Late Cretaceous and Cenozoic Mammals of North America*, Columbia University Press, New York , p. 156–168.
- Prothero, D. and Swisher, C., 1992, Magnetostratigraphy and geochronology of the terrestrial Eocene-Oligocene Transition in North America, *in* Prothero, D.R., Berggren, W.A. (Eds.), *Eocene–Oligocene Climatic and Biotic Evolution*. Princeton University Press, Princeton, NJ, p. 74-87.
- Retallack, G.J., 1983, Late Eocene and Oligocene paleosols from Badlands National Park, South Dakota: *Geological Society of America Special Paper 193*, p. 1–82.

- Retallack, G.J., 1992, Paleosols and change in climate and vegetation across the Eocene-Oligocene boundary, *in* Prothero, D.R., Berggren, W.A. (Eds.), *Eocene–Oligocene Climatic and Biotic Evolution*, Princeton University Press, Princeton, NJ, p. 116– 130.
- Retallack, G.J., 1997, *A colour guide to paleosols*, Chichester, Wiley, p.113-127.
- Retallack, G.J., 2005, Pedogenic carbonate proxies for amount and seasonality of precipitation in paleosols: *Geology*, v. 33, p. 333-336.
- Retallack G.J., 2007, Cenozoic paleoclimate on land in North America: *The Journal of Geology*, v. 115, p. 271-294.
- Sahy, D., Fischer, A., Terry, D.O., Jr., Condon, D., and Kuiper, K, 2010, Radio-Isotopic dating of volcanic ash layers from the White River Group, Wyoming and Nebraska: *Geological Society of America, Abstracts with Programs*, v. 42, p. 18.
- Schultz, C.B., and Stout, T.M., 1955, Classification of Oligocene sediments of Nebraska: *Bulletin of the University of Nebraska State Museum*, v. 4, p. 17-52.
- Sheldon N.D., 2009, Nonmarine records of climate change across the Eocene-Oligocene transition: *Geological Society of America Special Paper 452*, p. 241-248.
- Sheldon, N.D., and Retallack, G, 2004, Regional paleoprecipitation records for the late Eocene and Oligocene of North America: *The Journal of Geology*, v. 112, p. 487-494.
- Sheldon, N.D., Mitchell, R.L., Collinson, M.E., and Hooker, J.J., 2009, Eocene-Oligocene transition and paleoclimatic and paleoenvironmental record from the Isle of Wight (U.K.): *Geological Society of America Special Paper 452*, p. 249-259.
- Sheldon, N.D., and Tabor, N.J., 2009, Paleoenvironmental and paleoclimatic reconstruction using paleosols: *Earth-Science Reviews*, v. 95, p. 1-52.
- Sheppard, S.F.M., Nielsen, R.L., and Taylor, H.P., 1969, Oxygen and hydrogen isotope ratios in clay minerals from porphyry copper deposits: *Economic Geology*, v. 64, p. 755-777.
- Smeck, N.E., 1973, Phosphorous: an indicator of pedogenetic weathering processes: *Soil Science*, v. 115, p. 199-206.
- Strömberg, C.A.E., 2004, Using phytolith assemblages to reconstruct the origin and spread of grass-dominated habitats in the Great Plains of North America during the late Eocene to early Miocene: *Palaeogeography, Palaeoclimatology, Palaeoecology*, v. 207, p. 239-275.

- Terry, D.O., Jr., 1998, Lithostratigraphic revision and correlation of the lower part of the White River Group: South Dakota to Nebraska: Geological Society of America Special paper 325, p. 15-35.
- Terry, D.O., Jr., 2001, Paleopedology of the Chadron Formation of northwestern Nebraska: implications for paleoclimatic change in the North American midcontinent across the Eocene-Oligocene boundary: *Paleogeography, Paleoclimatology, Paleoecology*, v. 168, p. 1-38.
- Terry, D.O., Jr., and Evans, J., 1994, Pedogenesis and paleoclimatic implications of the Chamberlain Pass Formation, Basal White River Group, Badlands of South Dakota: *Journal of Sedimentary Geology*, v. 110, p. 197-215.
- Terry, D.O., Jr., and LaGarry, H., 1998, The Big Cottonwood Creek Member: A new member of the Chadron Formation in northwestern Nebraska: Geological Society of America Special paper 325, p. 117-141
- USDA Soil Survey Staff, 2010, *Soil taxonomy: Basic system of soil classification for making and interpreting soil surveys*, 2ed.: U.S. Department of Agriculture, p. 871.
- Whitlock, C. and P.J. Bartlein, 1993, Spatial variations of Holocene climatic change in the Yellowstone region: *Quaternary Research*, v. 39, p. 231-238.
- Wolfe, J.A., 1978, A paleobotanical interpretation of Tertiary climates in the northern hemisphere: *American Scientist*, v. 66, p. 694-703.
- Zanazzi, A., Kohn, M., Terry, D., 2009, Biostratigraphy and paleoclimatology of the Eocene-Oligocene boundary at Toadstool Park, northwestern Nebraska, USA: Geological Society of America Special Paper 452, p. 197-214.
- Zanazzi, A., 2008, Abrupt late Eocene climate change in North American Mid-Continent: Geological Society of America, Abstracts with Programs, v. 40, p.258
- Zanazzi, A., Kohn, M., MacFadden, B., Terry, D.O., 2007, Large temperature drop across the Eocene-Oligocene transition in central North America: *Nature*, v. 445, p. 639-642.
- Zachos, J., Pagani, M., Sloan, L., Thomas, E., and Billups, K., 2001, Trends, rhythms, and aberrations in global climate 65 MA to present: *Science*, v. 292, p. 686-693.

APPENDIX

Geochemical Data

Tipps Trench Paleosol Geochemistry

cm from top	-100	-90	-80	-70	-60	-50	-40	-30	-20	-10	0
Specimen	TT-1	TT-2	TT-3	TT-4	TT-5	TT-6	TT-7	TT-8	TT-9	TT-10	TT-11
SiO ₂	1.218	1.220	1.208	1.208	1.175	1.206	1.222	1.210	1.212	1.241	1.244
TiO ₂	0.008	0.008	0.008	0.008	0.008	0.008	0.008	0.008	0.008	0.008	0.008
Al ₂ O ₃	0.135	0.133	0.135	0.133	0.137	0.135	0.133	0.134	0.133	0.134	0.133
Fe ₂ O ₃ T	0.029	0.030	0.033	0.034	0.037	0.034	0.030	0.033	0.031	0.021	0.021
MnO	0.000	0.000	0.000	0.000	0.000	0.000	0.000	0.000	0.000	0.000	0.000
MgO	0.057	0.057	0.058	0.057	0.063	0.060	0.054	0.055	0.057	0.053	0.051
CaO	0.021	0.021	0.022	0.023	0.027	0.022	0.020	0.022	0.024	0.021	0.021
Na ₂ O	0.025	0.024	0.023	0.024	0.032	0.023	0.025	0.025	0.025	0.028	0.030
K ₂ O	0.027	0.026	0.026	0.027	0.027	0.026	0.026	0.027	0.026	0.026	0.026
P ₂ O ₅	0.001	0.001	0.002	0.002	0.003	0.002	0.001	0.001	0.002	0.001	0.001
Total	99.54	99.73	99.85	99.41	99.41	99.66	99.33	99.49	99.35	99.42	99.37
Rb	95.7	94.8	94.6	96.1	101.8	97	94.3	95.1	95.2	88.6	88.6
Sr	193	187	199	184	194	192	180	179	176	198	247
Y	27.8	25	27.7	29	34.4	28.2	22.6	23.7	28.1	23.5	26.2
Zr	324	342	330	331	323	351	357	324	355	365	374
V	72	66	77	78	74	70	91	55	71	74	73
Ni	19	19	20	21	21	20	19	19	20	19	19
Cr	68	69	68	67	75	78	78	84	68	70	67
Nb	14.1	13.2	14.1	13.8	14.4	14	13.1	13.3	13.6	12.1	12.2
Ga	14.6	13.7	14.4	14.7	15.3	14.7	14.5	14.3	14.9	14.8	15
Cu	18	15	17	26	17	15	23	13	37	15	14
Zn	52	49	49	52	55	50	47	47	51	49	48
Co	8	8	8	7	8	7	7	8	9	6	7
Ba	419	409	419	393	401	407	419	410	422	429	432
La	42	41	38	40	46	37	37	36	38	36	41
Ce	94	79	82	86	91	84	74	77	79	83	90
U	2.6	2.7	2.4	2.3	2.3	3.3	2.9	3.2	3.2	6.2	5.7
Th	15	12.5	13.6	15.3	14.5	14.6	17	14.3	14	13.9	13.8
Sc	10	9	9	10	9	10	10	9	10	10	11
Pb	29	25	23	25	23	25	22	22	26	33	34
Bases/Alumina	0.9606858	0.9593796	0.9675191	0.9825621	1.084341	0.9717811	0.9426188	0.972352	0.990392	0.962258	0.961305
Ba/Sr	2.1709845	2.1871658	2.1055276	2.1358696	2.0670103	2.1197917	2.3277778	2.290503	2.397727	2.166667	1.748988
MAP ₁	N/A	N/A	962.3	947.0	876.9	966.9	959.7	942.9	939.0	N/A	N/A
MAT ₁	N/A	N/A	10.4	10.3	9.4	10.6	10.1	10.0	10.2	N/A	N/A
MAT ₂	N/A	N/A	N/A	N/A	N/A	N/A	N/A	N/A	N/A	N/A	N/A

Ash A Paleosol Geochemistry										
cm from top	-90	-80	-70	-60	-50	-40	-30	-20	-10	0
Specimen	FR 2-1	FR 2-2	FR 2-3	FR 2-4	FR 2-5	FR 2-6	FR 2-7	FR 2-8	FR 2-9	FR 2-10
SiO ₂	0.868	1.122	1.094	1.146	1.084	1.042	1.045	1.131	1.162	1.179
TiO ₂	0.004	0.007	0.007	0.007	0.007	0.006	0.006	0.007	0.007	0.007
Al ₂ O ₃	0.100	0.133	0.129	0.135	0.130	0.124	0.122	0.134	0.135	0.134
Fe ₂ O ₃ T	0.019	0.025	0.027	0.028	0.027	0.025	0.026	0.028	0.027	0.025
MnO	0.002	0.001	0.001	0.001	0.001	0.001	0.001	0.001	0.001	0.001
MgO	0.037	0.048	0.053	0.057	0.056	0.053	0.052	0.058	0.057	0.051
CaO	0.501	0.123	0.162	0.088	0.171	0.235	0.236	0.106	0.069	0.058
Na ₂ O	0.032	0.039	0.033	0.033	0.031	0.031	0.032	0.033	0.033	0.037
K ₂ O	0.024	0.032	0.029	0.030	0.029	0.029	0.028	0.031	0.032	0.033
P ₂ O ₅	0.001	0.001	0.001	0.001	0.001	0.001	0.001	0.001	0.001	0.001
Total	100.340	99.400	100.110	99.570	100.320	100.240	99.370	99.350	99.470	99.740
Rb	87	119.7	112.7	118.3	113.1	111.8	110.2	118.3	124	123.5
Sr	202	234	247	267	236	264	242	258	263	280
Y	26.8	29.6	23.4	25.2	23.4	26.1	26.2	24.3	23.8	23.7
Zr	118	150	156	154	151	152	148	166	168	190
V	72	81	88	81	80	71	77	73	60	68
Ni	14	16	18	18	18	18	17	19	18	17
Cr	36	38	51	53	39	35	50	47	46	49
Nb	13.1	18	16	16.5	15.4	15.2	15.2	17.1	17.3	17.2
Ga	10.3	15.5	14.7	15.7	14.4	14.5	14.2	15.4	15.6	14.9
Cu	11	15	17	16	22	16	16	17	16	17
Zn	52	68	75	70	65	72	69	73	74	70
Co	4	7	7	7	7	8	9	9	8	6
Ba	371	568	569	599	544	527	521	587	680	860
La	23	27	27	28	27	27	29	28	26	29
Ce	39	57	50	65	61	62	54	67	67	69
U	4.5	5.8	4.6	5.1	3.9	5.4	4.8	5.3	4.4	5.7
Th	9.3	12.6	12.4	12.1	14	13.3	10.1	13.3	13.7	13.1
Sc	27	14	15	13	16	15	15	13	12	10
Pb	6	26	21	23	21	19	19	23	23	23
Bases/Alumina	5.939671	1.820141	2.14222	1.54774	2.202507	2.800583	2.84606	1.696213	1.413121	1.33089
Ba/Sr	1.836634	2.42735	2.303644	2.243446	2.305085	1.996212	2.152893	2.275194	2.585551	3.071429
MAP ₁	N/A	N/A	N/A	N/A	N/A	414.0	410.0	583.0	N/A	N/A
MAT ₁	N/A	N/A	N/A	N/A	N/A	8.4	8.2	8.5	N/A	N/A
MAT ₂	N/A	N/A	N/A	N/A	N/A	9.6	9.6	9.5	N/A	N/A

Ash F Paleosol Geochemistry

cm from top	-80	-70	-60	-50	-40	-30	-20
Specimen	FR3-4	FR3-5	FR3-6	FR3-7	FR3-8	FR3-9	FR3-10
SiO ₂	1.13	1.15	1.14	1.14	1.19	1.09	1.11
TiO ₂	0.01	0.01	0.01	0.01	0.01	0.01	0.01
Al ₂ O ₃	0.15	0.14	0.14	0.14	0.14	0.14	0.14
Fe ₂ O ₃ T	0.03	0.03	0.03	0.03	0.02	0.03	0.03
MnO	0.00	0.00	0.00	0.00	0.00	0.00	0.00
MgO	0.07	0.08	0.08	0.08	0.06	0.08	0.07
CaO	0.06	0.06	0.08	0.07	0.05	0.12	0.11
Na ₂ O	0.03	0.02	0.02	0.02	0.03	0.02	0.02
K ₂ O	0.03	0.03	0.03	0.03	0.03	0.03	0.03
P ₂ O ₅	0.00	0.00	0.00	0.00	0.00	0.00	0.00
Total	99.96	100.01	99.47	99.61	99.91	100.61	100.44
Rb	108.3	109.9	119.0	116.7	114.4	117.3	104.4
Sr	333	288	279	273	318	275	328
Y	23.6	21.7	22.8	32.1	17.6	21.2	23.5
Zr	207	177	161	163	227	163	215
V	87	82	78	85	74	72	74
Ni	21	21	22	22	17	23	21
Cr	61	68	56	49	51	54	55
Nb	14.9	14.2	14.6	14.7	14.9	15.4	14.2
Ga	15.6	15.8	15.7	16.0	14.7	16.0	15.2
Cu	21	24	26	25	12	24	19
Zn	80	88	86	90	83	93	81
Co	8	9	11	10	6	10	8
Ba	611	566	621	538	703	535	598
La	33	31	33	39	28	31	32
Ce	75	70	75	96	57	69	80
U	4.7	4.3	3.4	2.7	3.6	4.5	4.2
Th	13.1	13.2	13.3	15.0	13.8	13.8	14.9
Sc	11	13	11	12	10	15	12
Pb	25	25	22	21	31	19	23
Bases/Alumina	1.295374	1.357581	1.463165	1.40966	1.209757	1.798157	1.688628
Ba/Sr	1.834835	1.965278	2.225806	1.970696	2.210692	1.945455	1.823171
MAP ₁	N/A	N/A	N/A	N/A	N/A	586.0	597.0
MAT ₁	N/A	N/A	N/A	N/A	N/A	10.7	10.3
MAT ₂	N/A	N/A	N/A	N/A	N/A	10.0	10.0

Ash J Paleosol Geochemistry

cm from top	-110	-100	-90	-80	-70	-60	-50	-40	-30	-20	-10	0
Specimen	FR 5-1	FR 5-2	FR 5-3	FR 5-4	FR 5-5	FR 5-6	FR 5-7	FR 5-8	FR 5-9	FR 5-10	FR 5-11	FR 5-12
SiO ₂	1.026	1.169	0.849	0.839	0.918	1.180	1.175	0.884	0.923	1.169	0.863	0.855
TiO ₂	0.006	0.007	0.005	0.005	0.005	0.007	0.007	0.004	0.005	0.007	0.004	0.004
Al ₂ O ₃	0.118	0.134	0.096	0.095	0.104	0.134	0.134	0.097	0.104	0.133	0.097	0.096
Fe ₂ O ₃ T	0.022	0.024	0.019	0.019	0.020	0.025	0.024	0.016	0.019	0.022	0.017	0.017
MnO	0.001	0.001	0.001	0.001	0.001	0.001	0.001	0.002	0.001	0.001	0.003	0.003
MgO	0.046	0.052	0.043	0.042	0.044	0.050	0.049	0.032	0.040	0.047	0.037	0.037
CaO	0.282	0.077	0.539	0.553	0.440	0.064	0.073	0.508	0.436	0.081	0.522	0.531
Na ₂ O	0.028	0.030	0.023	0.022	0.025	0.030	0.030	0.025	0.027	0.034	0.028	0.028
K ₂ O	0.030	0.034	0.024	0.023	0.026	0.034	0.034	0.027	0.027	0.036	0.026	0.026
P ₂ O ₅	0.001	0.001	0.001	0.001	0.001	0.001	0.001	0.001	0.001	0.001	0.001	0.001
Total	99.89	100.11	99.6	99.48	99.53	100.08	100.19	99.46	99.56	99.75	99.67	99.5
Rb	93.90	111.00	74.20	71.20	77.80	109.10	110.10	83.80	83.40	116.70	91.30	80.50
Sr	279	317	262	250	270	305	311	234	237	288	237	236
Y	23.1	20.9	23.6	23.7	25.7	20.6	21.3	19.9	24.7	24.6	21.2	23.5
Zr	219	265	198	198	203	260	255	176	212	253	195	180
V	64	82	52	53	61	87	80	37	60	64	48	47
Ni	15	17	14	13	15	18	17	10	14	15	14	13
Cr	32	43	29	22	26	45	47	16	24	39	24	20
Nb	11.3	13.4	9.1	9.1	9.4	13.6	13.4	9.1	10.3	14.3	10.6	9.4
Ga	12.8	14.3	10	8.8	10.9	14.8	15	9.1	10.3	14.7	10.7	9.6
Cu	20	21	18	15	16	22	19	9	13	17	13	11
Zn	67	71	58	53	58	70	68	46	53	67	54	51
Co	7	7	6	5	6	9	7	1	3	6	5	3
Ba	683	804	414	359	523	798	863	545	404	637	496	349
La	25	28	27	23	29	30	30	25	26	32	26	25
Ce	59	73	43	39	46	83	79	45	42	70	44	46
U	4	3.7	2.6	2.5	2.4	4.1	3.9	3.5	3	4.1	3.3	2.7
Th	8.7	12.9	6.5	6.7	6.2	11.8	10.6	9.7	7.4	13.1	8.1	8.4
Sc	16	11	26	25	22	12	13	20	26	12	22	25
Pb	13	19	5	3	7	20	18	3	5	19	6	4
Bases/Alumina	3.278029	1.449098	6.5269	6.78003	5.149522	1.337681	1.395625	6.08116	5.083242	1.487113	6.343555	6.444446
Ba/Sr	2.448029	2.536278	1.580153	1.436	1.937037	2.616393	2.77492	2.32906	1.704641	2.211806	2.092827	1.478814
MAP ₁	N/A	N/A	295.0	292.0	317.0	N/A	N/A	N/A	N/A	N/A	N/A	N/A
MAT ₁	N/A	N/A	8.4	8.3	8.3	N/A	N/A	N/A	N/A	N/A	N/A	N/A
MAT ₂	N/A	N/A	9.3	9.3	9.3	N/A	N/A	N/A	N/A	N/A	N/A	N/A